

Reply to Reviewer (1)'s comments on gmd-2016-150

[We would like to thank the reviewer for the valuable comments and suggestions.](#)  
[Here are our responses to the reviewer's comments.](#)

Comments to author:

Ensemble forecasts are produced as the routine products in many NWP operational centers. Using these products to estimate uncertainties is convenient and becomes popular.

This paper employed PF method, where the ensemble data is used to estimate cloud fraction, to retrieve cloud. The PF method provided improvements on the accuracies of cloud retrieval, i.e. cloud profile, cloud mask and cloud top, and also made the cost cheaper. This action is meaningful. Glad to see the study when satellite data is increasing in volume and plays the important role in providing extra information in NWP and data assimilation systems.

The extension of PF method to the cloud data retrieval is, I think, a good contribution to the application of cloud products and a good addition to the literature. However, I see some deficiencies or ambiguous sentences in the paper that lead me to suggest major revisions before it is published. I see three major points that need to be corrected or explained.

1) The probabilities of the cloud distribution are presented by the initial particles. Thus, a particle initialization scheme is needed. Authors firstly generated the perturbations of cloud fractions by inflating, deflating and moving the clouds. My question is: (a) why did authors generate perturbations of cloud fractions when the cloud fractions were actually available among the ensemble members? Or say, why not use cloud fraction in ensemble members directly to generate the particles? If authors argue that the ensemble spread of cloud fractions in ensemble dataset is not large enough, it is reasonable but some statements should be stated here. (b) Did authors use any method and rule in this study to inflate, deflate and move the cloud? Some random perturbations might be deficient, and accounting for different

perturbation methods could very well change some of the results in the basic PF experiment. I get the conclusion partly from Fig.4, where the cloud fraction is obviously different between PF and APF and thus the different cloud retrievals are produced.

-----

Reply: Basically, two groups of initial particles are used to retrieve the clouds in PF in this study. The first group includes particles that adding perturbations to clouds in the background in warm starts to further utilize prior information. The second group is to generate one-layer cloud on each model level with an even chance using different numbers of samples (e.g., with 100% interval, 10% interval, and 1% interval). There are two motivations of using the first group particles in addition to the particles in the second group. 1) Although cloud fractions can be actually retrieved with enough particles in group 2 with 1% interval, the computational cost is high, whereas the spread from particles with 10% or 100% intervals is not enough. 2) Since clouds move and evolve continuously in most cases, it may be more efficiently to generate a group of particles based on the warm background.

To make it clear, we added more explanations and statements as “The perturbed cloud fractions are designated to replenish the ensemble by introducing the prior information of the cloud distributions from the background and to increase the ensemble spread.” and “the first one is to generate the perturbed samples  $C_b^i$  (  $\forall i \in [1, n]$  ) from the cloud profile in the background denoted as  $C_b = (c_b^0, c_b^1, \dots, c_b^K)$  by inflating (deflating) the clouds with small magnitudes (  $C_b = \alpha \times C_b, \alpha = 50\%, 55\%, \dots, 150\%$  ) and moving upward (downward) with  $\delta z = +5, +4, \dots, -1, \dots, -5$  as the vertical magnitude, where  $n$  is the sample size.” in section 1.

2) L174-175. “Generally, for each FOV, the retrieved cloud fractions are extrapolated

to its four neighboring model grid points”. What method is employed by authors to do the extrapolation from one cloud fraction to its neighboring grid points? Compared with the interpolation from background to FOV, which is a routine way to calculate the residual, is there any chance to make accuracy loss of radiance observations by the extrapolation? If so, how the loss of accuracy affects the weight in Eq. 3? I think authors need to tell the reader in more detail about this.

-----

Reply: Since the final retrieval clouds are on model grids, the retrieved cloud fractions within one FOV are essentially extrapolated to its four neighboring model grid points. Especially, for polar satellite pixels, the representative cloud fractions are extrapolated with an adaptive radius with respect to their scan positions. Since the clouds are retrieved FOV by FOV and the clouds on grids are referred immediately after one FOV is completed, there is no obvious accuracy loss of radiance observations using this conservative method. To make it clear, we added more related explanations and statements in the first paragraph in section 3.3.

3) It is not a real question here. It is fine to use 150 hPa as the highest extent in this study. However, in reality, the tropopause could be higher than 150 hPa, e.g. an anvil cloud in a mature thunderstorm around tropopause at low latitude region. The fact can be also found out in Fig.4, where the cloud fraction around 150 hPa is not zero in the experiment ‘PF’. I do not ask authors to run extra experiments to estimate cloud fraction on all model levels because the cloud fraction is too small above 150 hPa and

I consider this less important in this study. I just would like to say that we should not omit any extreme weather when we have the ability to resolve it.

-----

Reply: We agree that in reality the tropopause could be higher than 150 hPa occasionally with very small probability. In fig. 4 (using the same y-axis with fig. 2), all the experiments are already conducted using 150 hPa as the highest extent. The reason that the averaged cloud fraction (cf) around 150 hPa is not exactly zero is that

the cf is strictly for each model level. The pressure levels on the right y-axis are estimated roughly using the domain averaged pressure. We agree that any extreme weather should not be omitted and thus we added more explanations and statements as “The MMR and PF cloud detection schemes search the cloud top using approximately 150 hPa as the highest extent for most cloudy cases. Other clouds higher 150 hPa, e.g. an anvil cloud in a mature thunderstorm around tropopause at low latitude region will also be explored in future studies.” in section 3.3 and “Increasing the highest extent cloudy cases will be included in future studies.” in the future plan.

That is a summary of my major concerns. The following are minor specific concerns generally relevant to specific portions of the text.

Line 13-16: If authors use the qualitative comments (L13-14) as the beginning, I suggest to add, say ‘by using ensemble forecasts/products’, behind PF in L15 to keep consistent to the L13-14. I don’t think that all of readers are familiar with Particle Filter in which the ensemble concept is implicit when they read the abstract firstly, although the PF is introduced in section 2.

-----  
Reply: A new cloud retrieval method is proposed based on the efficient Particle Filter (PF) by using ensembles of cloud information in the framework of Gridpoint Statistical Interpolation system (GSI).

L48-50: Check parenthesis and comma, which do not match.

-----  
Reply: Corrected.

L98-101: Is  $c_0$  constant, if it is not the control variable?

-----  
Reply:  $c^0$  is one of the control variables in the cost function of MMR, instead of a constant. We add more explanations as “ The residual of the modeled radiance and

the observation is normalized by the observed radiance, which results in the following cost function, using  $c^k$ ,  $\forall k \in [0, K]$  as the control variables”

L101-102: Might state how  $R_v^k$  is calculated briefly, e.g by forward CRTM operator with the inputs of temperature and humidity profiles in background.

-----  
Reply: Accepted. We add statements as “Both  $R_v^k$  and  $R_v^o$  are calculated using a forward radiative transfer model with model profiles of temperature and moisture as inputs.” in the first paragraph of section 2.

L107: Suggest to note that the ‘particles’ correspond with ‘ensemble members’, i.e. one cloud profile as one of particles is derived from an ensemble member.

-----  
Reply: Accepted. We add “Explicitly, the definition of particles corresponds with ensemble members, i.e. one cloud profile as one of particles is corresponding to an ensemble member.” in the fourth paragraph of section 2 to state the definition of particles clearly.

L131: If the observation error in Eq. 3 is specified in GSI, please state it.

-----  
Reply: Here  $p$  is the particle size and  $\sigma$  is the specified observation error, which can be referred in the first paragraph in section 4.1.

L152: Only GOES-13 and -15 used in this study? Does not match with Fig. 4.

-----  
Reply: The sentence is revised as “In this study, GOES-13 (east) and GOES-15 (west) are also utilized to obtain cloud fractions over the continental United States (CONUS) domain.”

L175: See major concern 2.

-----  
Reply: See detailed reply to the above second major points of comments.

L189-196: Do authors implement bias correction for these satellite cloud products as reference?  
-----

Reply: No. That's why we utilized multiple cloud products for comprehensively comparisons.

L202: Should be Eq. 3.  
-----

Reply: Corrected. Since we added two new equations in ahead of Eq. (3), Eq. (3) is labelled as Eq. (5) in the revised manuscript.

L216: Title of x-axis missed. Also check Fig. 2(c)(d).  
-----

Reply: Done.

L221 and L236: From Fig. 2a, I think the results are produced by using PF, because authors use these words "specified value of cloud fractions". However, the "normalized J0" is showed in Fig. 2c. It is confusing because MMR employs the cost function. If J0 is the residual in Eq. 3, please state it clearly.  
-----

Reply: Yes. Fig. 2ab and Fig. 2cd are all using PF. We add more explanations in the sixth paragraph in section 2 as "A cost function Jo is defined for each particle to measure how the particle fit the observation as,

$$J_o = \left( \frac{R_v^{\text{obs}} - R_{v,j}^{\text{cloud}}}{\sigma} \right)^2 \quad (4)$$

" to state it clearly.

L249: Fig. 2 could be separated into two figures, cloud fraction Fig. 2(a) (b) and

normalized J0 Fig. 2(c)(d).

---

Reply: Done.

L293: I guess authors use AIRS as Robs to calculate residual, but need to re-write the word “from AIRS”.

---

Reply: Corrected. We re-write as “with AIRS observations”.

L372: Keep the units consistent. Check Fig. 9 and Fig. 10. Use (hour) or (hr), not (hh).

---

Reply: Corrected.

Reply to Reviewer (2)'s comments on gmd-2016-150

We would like to thank the reviewer for careful and thorough reading of this manuscript and for the constructive suggestions. Here are our responses to the reviewer's comments.

Comments to author:

General comments:

The aim of the paper is to introduce a new retrieval cloud method, based on the particle filter approach. Since several very different configuration of cloud can lead to the same observed radiance, PF appears as nice tool for this problem. While similar use of the PF have been introduced in other domains (see comment 1 below), this is a new applications in this fields. The proposed method is compared with state of the art

(MMR) where several particle generating techniques have been considered. The results are well presented with an pedagogical situation to explore the potential of the method, and real cases. The benefit of the PF are a better retrieval at a lower cost compared with the MMR. The manuscript can be improved to facilitate its reading following the comments, and minor revision are required.

Comments:

1) The bibliography on PF focuses on classical data assimilation consideration to estimate initial state. However, PF can also be used to parameter estimation or disaggregation which is similar to what introduced here, see eg Mechri et al. (2015). Hence you should clearly state the difference between the use of PF in classical DA and the present one, even if this relies on the same formalism, and improve the bibliography on this aspect.

-----  
Reply: We reorganized the methodology part and added statements as "Particle filter (PF) approach is one of the nonlinear filters for data assimilation procedures to best estimate the initial state of a system or its parameters  $x_t$ , which describes the time



evolution of the full probability density function  $p(x_i)$  conditioned by the dynamics and the observations. Similar to (Mechri et al., 2014), the bibliography on PF focuses on estimating the parameters, which are the cloud fractions  $c^k$  in Eq. (3), in this study.” in paragraph 3 in section 2.

2) Par 1, sec 2, L82: Precise the idea of cloud retrieval: this is implicit but for self consistency it is better to explain (generation of radiance from model, compared with observation, if they match then the cloud structure is found).

-----  
Reply: Agreed. More statements are added as “Both cloud retrieval schemes consist of finding cloud fractions that allow best fit between the cloudy radiance from model and the observation.” in the first paragraph in section 2.

3) L87: Precise the level associated with upper script  $k$  ( $k=1$  means near the surface .. or top atmosphere as encountered in NWP models – Fig. 1 explains it corresponds to the surface, but this should be written) ?

-----  
Reply: Accepted. In the revised manuscript, “We use  $c^1, c^2, \dots, c^K$  to denote the array of vertical effective cloud fractions for  $K$  model levels ( $c^1$  for the surface and  $c^K$  for the model top) and  $c^0$  as the fraction of clear sky with  $0 \leq c^k \leq 1, \forall k \in [0, K]$ .” in section 2.

4) L87: “effective” is not clear, it should be better to explain as the fraction of top of cloud as seen from a sensor.

-----  
Reply: Accepted. We revised the statements as “Essentially, the PF cloud retrieval scheme retrieves clouds with the same critical inputs requested (i. e., clear sky radiance from the radiative transfer model and the observed radiance) and the same

cloud retrievals as outputs (i. e., three dimensional cloud fractions, which is defined as the fraction of top of cloud as seen from a sensor) with the MMR method.” in place of effective three dimensional cloud fractions).

5) L88: Following the previous point 4), with the condition  $0 \leq c^k \leq 1$ , precise that

$\sum_{k=0}^K c^k = 1$  at this place, with a label for this equation (the sum can be suppressed from L101).

-----

Reply: Agreed. We labelled the equation and suppressed the sum from L101.

6) L111: the definition of what is a particle is crucial since it use to be model state in classical dynamical system that is not the case here. Hence, you should precise explicitly that P stands for the vector  $\mathbf{c} = (c^0, c^1, \dots, c^K)$ . In the notation, P can be interpreted as a function ck.. I think better to use  $\mathbf{C} = (c^0, c^1, \dots, c^K)$  for the particle in place of the notation P that could lead to confusion with the probability notation underlined with the particle filter approach. (see point 13 below)

-----

Reply: Accepted. We adopted the reviewer’s idea that using  $\mathbf{C} = (c^0, c^1, \dots, c^K)$  to interpret the particle, which makes the notations more clear.

7) L113: “typical” provide reference to previous work showing the method is known or suppress “typical”.

-----

Reply: Agreed. We deleted “typical” in the sentence.

8) L115: add an subscript b to  $c^k$  in  $P_b$  as  $c_b^k$

-----

Reply: Done.

9) L115: “inflating, deflating, moving” should be illustrate using a regular 2D mesh, a simple figure would illustrates the fact that moving can suppress some fraction (a cloud becoming masked by another at upper level).

-----

Reply: Done. The first one is to generate the perturbed samples  $C_b^i$  (  $\forall i \in [1, n]$  ) from the cloud profile in the background denoted as  $C_b = (c_b^0, c_b^1, \dots, c_b^K)$  by inflating (deflating) the clouds with small magnitudes (  $C_b = \alpha \times C_b, \alpha = 50\%, 55\%, \dots, 150\%$  ) and moving upward (downward) with  $\delta z = +5, +4, \dots, -1, \dots, -5$  as the vertical magnitude, where n is the sample size.

10) L111-126: the two approaches (L113) are not clearly separated, make two different paragraph one for each method (L114: the perturbation; L120 L123 the full/fractional one level top cloud)

-----

Reply: Accepted.

11) L126: precise that for one-layer cloud at level i, the clear sky fraction is  $c^0 = 1 - c^i$

-----

Reply: Accepted.

12) L130: Eq.(3) means the comparison is done for one frequency.. what happens with other frequency (robustness, sensitivity) ? MMR relies on multiple frequency. At the opposite the PF seems to be used with only one. Please clarify this point / explain more precisely what is done.

-----

Reply: PF also is conducted based on multiple frequency. We revised the manuscript as “The weight  $w^i$  for each particle  $C_b^i$  thus is calculated by comparing the simulated  $R_{v,i}^{\text{cloud}}$  and the observation  $R_v^{\text{obs}}$  using the exponential function by accumulating the Jo for multiple frequency as

$$w^i = e^{-\sum_v \left( \frac{R_v^{\text{obs}} - R_{v,i}^{\text{cloud}}}{\sigma} \right)^2}, \quad (5)$$

$\forall i \in [1, p]$ .” in sixth paragraph in section 2.

13) L134: with the notation C, Eq.(4) becomes  $C_a = \sum_{i=1}^p w^i P_b^i$  which is less confusing than with notation P.

-----  
Reply: Accepted.

14) L135: what is mean by updating ? (resampling strategy? analysis step?) I guess you mean analysis step for the particule filter, this should be clarified.

-----  
Reply: Corrected. The revised sentence is “After the analysis step for the particle filter, the final averaged cloud fractions...”

15) L135: precise that the average cloud fraction is no more normalised since the constraint (equation labelled from the above comments point 5) is not respected from the average Eq.(4) – average of state is no more a real state.

-----  
Reply: Agreed. We added statements as “In Eq. (6), the constraint referred in Eq. (1) is not respected. Thus, after the analysis step for the particle filter, the final averaged cloud fractions  $C_a^k$  are normalized by...”

16) L202: Eq.(7) --->Eq.(3)

-----  
Reply: Corrected. Since we added two new equations in ahead of Eq. (3), Eq. (3) is labelled as Eq. (5) in the revised manuscript.

17) L203: modify the notation for the prescribed ratio o\_f is meaningless (use r, or something else, or explain why this notation is used).  
-----

Reply: Agreed.

We re-wrote the sentence as “In Eq. (3), the observation error  $\sigma$  can be set proportional to the observation, equaling to  $\frac{R_v^{obs}}{r}$ , where  $r$  is the prescribed ratio.” in the revised manuscript.

18) L221-224: The particle used there corresponds to the groupe2 described previously, this should be reminded.  
-----

Reply: Agreed.

In second paragraph of section 4.1., we added explanations of particles as “To reveal the roles of various initial particles, Fig. 2a shows the weights for different particles of one-layer cloud in group 2 described in section 2 with specified value of cloud fractions (on the x-axis) on specified model levels (on the y-axis) from 10% to 100% every 10% on the given FOV for channel 5 of GOES-Imager for the case shown in Fig. 1.”

19) L224: Detail that the observation can be explained by different possible state and in particular as a fraction  $c^i$  of one-cloud layer at a given level i and a fraction of  $c^0 = 1 - c^i$  of clear sky since  $R_v^{cloud} = c^i R_v^i + (1 - c^i) R_v^0$  for levels i upper than level 5. Hence the theoretical one-layer cloud fraction is the solution of

$R_v^{obs} = c^i R_v^i + (1 - c^i) R_v^0$  that is by  $c^i = \frac{R_v^0 - R_v^{obs}}{R_v^0 - R_v^i}$ . No cloud can be present below

level 5 since this would implies an  $R_v^{cloud}$  larger then the observation (or a  $c^i$  larger than 100%). Provide a representation of the theoretical one-layer fraction so to introduce Fig2. This said, it is then easier to conclude that the weight in Fig2a 2b reproduce these possible situation with a maximum weight concentrated when the fraction is near the theoretical one given above.

-----

Reply: Accepted. We add theoretical representation in the second paragraph in section 4.1 as “With a fraction  $c^k$  of one-cloud layer at a given level k and a fraction of  $c^0 = 1 - c^k$  of clear sky, the simulated cloudy radiance can be denoted as  $R_v^{cloud} = c^k R_v^k + (1 - c^k) R_v^0$ . Hence the theoretical one-layer cloud fraction is solved as  $c^k = \frac{R_v^0 - R_v^{obs}}{R_v^0 - R_v^k}$  by fitting  $R_v^{cloud}$  to  $R_v^0$ . As expected, for one-layer cloud with full fraction,  $c^5$  equals to 100%. Since with the concept that  $R_v^k > R_v^{k+1}$ , no cloud can be present below level 5 since this would implies a  $R_v^{cloud}$  larger than the observation (or a  $c^i$  larger than 100%).”

20) L236: What is the normalized Jo ? I guess this should corresponds to the exponent in Eq.(3), but this is not introduced before. Provides the expression of Jo as a function of cloud fraction, it will be easier to understand what represents Fig. 2(c-d), when  $C^k = (0, ..., c^k, 0, ..., 0)$  with  $c^k$  set to 0, 0.1, ..., 1 (c) and ... (d)

-----

Reply: Agreed. We add more explanations in section 2 as “A cost function Jo is defined for each particle to measure how the particle fit the observation as,

$$J_o = \left( \frac{R_v^{\text{obs}} - R_{v,d}^{\text{cloud}}}{\sigma} \right)^2 \quad (4)''$$

and also add sentence in section 4.1 as “Here, Jo can be further derived as

$$J_o = r^2 \left( 1 - c^0 \frac{R_v^0}{R_v^{\text{obs}}} - c^i \frac{R_v^i}{R_v^{\text{obs}}} \right)^2 \quad (8),$$

with  $\sigma = \frac{R_v^{\text{obs}}}{r}$  and  $R_v^{\text{cloud}}(c^0, c^1, c^2, \dots, c^K) = c^0 R_v^0 + \sum_{k=1}^K c^k R_v^k$ .”

References:

Mechri, R.; Ottele, C.; Pannekoucke, O. Kallel, A. Genetic particle filter application to land surface temperature downscaling Journal Geophysical Research: Atmospheres, 2014, 119, 2131-2146

Reply to Reviewer (1)'s comments on gmd-2016-150

We would like to thank the reviewer for further reading through this manuscript and comments to improve this manuscript. Here are our responses.

Comments to author:

The authors have done some work to appropriately address my remarks and provide answers. The relevant discussion was also included at several places throughout the manuscript. I therefore recommend the manuscript be accepted for publication once the authors make the following typos that should still be considered.

L15: May delete 'efficient'.

-----  
Reply: Agreed.

L39: Consider using 'remote sensing of earth' instead of 'earth remote sensing'.

-----  
Reply: Accepted.

L51: May use [ ] instead of the outer ().

-----  
Reply: Agreed.

L66: May use 'various' or other words instead of 'all kinds of' ?

-----  
Reply: Agreed. The revised sentence is "...in diversified forms (Snyder and Zhang, 2003), have been widely developed in order to estimate the uncertainties of various problems in geophysical applications."

L118: Similar to the study (or implementation ) in Mechri et al.....

-----  
Reply: Corrected. The sentence is revised as "Similar to the study in Mechri et al.....".

L125: May delete 'Explicitly'.

-----  
Reply: Accepted.



L136: The equation never happens in mathematic unless  $\alpha$  is 1. May use another letter for the left  $C_b$ .

-----  
Reply: Corrected. We modified the equation as  $C_b^i = \alpha \times C_b, \alpha = 50\%, 55\%, \dots, 150\%$ .

L150: Eq.2  $\rightarrow$  Eq. 3

-----  
Reply: Done.

L154: Move the definition of  $\sigma$  at L158 to this line.

-----  
Reply: Accepted.

L158: Is n at L137 the same as p at L158 ? If so, why not use the same letter, n or p ?

-----  
Reply: Corrected. We used n consistently in the revised manuscript.

L255: The sentence is too long. Rewrite it.

-----  
Reply: We re-organized the sentence as two separate sentences.

L297: Fig. 2 looks fine. However, cloud fraction and Normalized Jo are not the same thing. It may be better to consider Normalized Jo as Fig. 3.

-----  
Reply: Agreed. We modified Fig. 2c and Fig. 2d to be Fig. 3a and Fig. 3b. The following Figure captions are also corrected accordingly.

**A method for retrieving clouds with satellite infrared  
radiances using the particle filter**

Dongmei Xu<sup>1,2</sup>, Thomas Auligné<sup>2</sup>, Gaël Descombes<sup>2</sup>, and Chris Snyder<sup>2</sup>

<sup>1</sup>[Key Laboratory of Meteorological Disaster, Ministry of Education \(KLME\) /Joint International Research Laboratory of Climate and Environment Change \(ILCEC\) /Collaborative Innovation Center on Forecast and Evaluation of Meteorological Disasters \(CIC-FEMD\), Nanjing University of Information Science & Technology, Nanjing 210044, China](#)

<sup>2</sup>National Center for Atmospheric Research, Boulder, Colorado 80301, USA

(2016/9/10)

Administrator 2016-08-08 10:37	✓	🔒
带格式的: 法语(法国)		
Administrator 2016-09-10 15:00	✓	🔒
删除的内容: y		
Administrator 2016-08-08 10:37	✓	🔒
带格式的: 法语(法国)		
anna 2016-07-30 20:16	✓	🔒
删除的内容: Collaborative Innovation Center on Forecast and Evaluation of Meteorological Disasters, Nanjing University of Information Science & Technology, Nanjing, 210044, China		
Administrator 2016-09-10 15:16	✓	🔒
删除的内容: 78		
anna 2016-08-11 07:21	✓	🔒
删除的内容: 30		
Administrator 2016-09-10 15:16	✓	🔒
删除的内容: 1		

**\* Corresponding Author**

Dr. Dongmei Xu  
Nanjing University of Information Science & Technology, College of Atmospheric science,  
Ningliu road, No. 219, Nanjing, 210044, China  
E-mail: [xdmjolly@sina.com](mailto:xdmjolly@sina.com)

## Abstract

Ensemble-based techniques have been widely utilized in estimating uncertainties in various problems of interest in geophysical applications. A new cloud retrieval method is proposed based on the Particle Filter (PF) [by using ensembles of cloud information](#) in the framework of Gridpoint Statistical Interpolation system (GSI). The PF cloud retrieval method is compared with the Multivariate and Minimum Residual (MMR) method that was previously established and verified. Cloud retrieval experiments involving a variety of cloudy types are conducted with the PF and MMR methods respectively with measurements of Infrared radiances on multi-sensors onboard both geostationary and polar satellites. It is found that the retrieved cloud masks with both methods are consistent with other independent cloud products. MMR is prone to producing ambiguous small-fraction clouds, while PF detects clearer cloud signals, yielding closer heights of cloud top and cloud base to other references. More collections of small fraction particles are able to effectively estimate the semi-transparent high clouds. It is found that radiances with high spectral resolutions contribute to quantitative cloud top and cloud base retrievals. In addition, a different way of resolving the filtering problem over each model grid is tested to better aggregate the weights with all available sensors considered, which is proven to be less constrained by the ordering of sensors. Compared to the MMR method, the PF method is overall more computationally efficient, and the cost of the model grid-based PF method scales more directly with the number of computing nodes.

Administrator 2016-09-10 15:17 ✓

删除的内容: efficient

23    Keywords: cloud retrieval methods, particle filter, GSI system, cloud height

## 1. Introduction

Modern polar orbiting and geostationary airborne instruments provide researchers unprecedented opportunities for remote sensing of earth with continuous flows and almost complete spectral coverage of data. The primary cloud retrieval products from satellites are cloud mask (CM), cloud height (CH), effective cloud fraction (CF), and vertical structures of clouds with larger temporal and spatial scales. These cloud retrievals provide an immense and valuable combination for better initializing hydrometeors in numerical weather prediction (NWP), (Wu and Smith, 1992; Hu et al., 2006; Bayler et al., 2000; Auligné et al., 2011) regulating the radiation budget for the planet, and understanding the climate feedback mechanism (Rossow and Schiffer, 1991; Rossow et al., 1993; Brückner et al., 2014). Advanced cloud retrieval methods are able to retrieve clouds with multispectral techniques (Menzel et al., 1983; Platnick et al., 2003), among which the minimization methods usually directly utilize the difference between the modeled clear sky and the observed cloudy Infrared (IR) radiances [e. g., the minimum residual method, (Eyre and Menzel, 1989); the Minimum Local Emissivity Variance method, (Huang et al., 2004); and the Multivariate Minimum Residual method, (Auligné, 2014a)]. Specially, the Multivariate Minimum Residual (MMR) method is retrieving three dimensional multi-layer clouds by minimizing a cost function at each field-of-view (FOV) (Auligné, 2014b; Xu et al., 2015). MMR has been proven to be reliable in retrieving the quantitative three dimensional cloud fractions with Infrared radiances from

Administrator 2016-09-10 15:17



删除的内容: earth

Administrator 2016-09-10 15:18



删除的内容: (

Administrator 2016-09-10 15:18



删除的内容: )

multiple infrared instruments. However, MMR has limitations in several aspects due to its use of minimization for solution: 1) Part of the control variables accounting for the cloud fraction for some certain levels are under-observed since the channels are not sensitive to the existence of clouds for those heights. 2) When clouds at different heights show opacities with the same spectral signal, MMR could lose the ability to distinguish solutions involving clouds at those levels. 3) The computational cost for the minimization procedure in MMR is rather considerable.

Ensemble-based techniques, that usually reside in short-term ensemble forecasting (Berrocal et al., 2007), assembling existing model outputs (e. g., cloud retrievals) from varying algorithms (Zhao et al., 2012), or ensemble Kalman filter (EnKF) in diversified forms (Snyder and Zhang, 2003), have been widely developed in order to estimate the uncertainties of various problems in geophysical applications.

To better account for the non-linearity between the observed radiance and the retrieval parameter, a novel prototype for detecting clouds and retrieving their vertical extension inspired by the particle filter (Snyder and Zhang, 2003; van Leeuwen, 2010; Shen and Tang, 2015) technique and Bayesian theory (Karlsson et al., 2015) is proposed in this study. As a competitive alternative for MMR, the PF retrieval method has same critical inputs required and cloud retrieval products as in MMR. A brief description of MMR and the new PF cloud retrieval algorithm are provided in the following section. Section 3 describes the background model, the data assimilation system, the radiative transfer models (RTMs), and the radiance observations applied in this study. Model configurations are also illustrated in

Administrator 2016-09-10 15:18	✓	🔒
删除的内容: various		
Administrator 2016-09-10 15:19	✓	🔒
删除的内容: all kinds of		

section 3. In section 4, the single test within one FOV is conducted before the performance of PF method is assessed by comparing its cloud retrievals with those from MMR and other operational cloud products. Section 4 also discusses the computational performance for the two methods. The conclusion and anticipated future work are outlined in section 5.

## 2. Methodology

Essentially, the PF cloud retrieval scheme retrieves clouds with the same critical inputs requested (i. e., clear sky radiance from the radiative transfer model and the observed radiance) and the same cloud retrievals as outputs (i. e., three dimensional cloud fractions, which is defined as the fraction of top of cloud as seen from a sensor) with the MMR method. Both cloud retrieval schemes consist of finding cloud fractions that allow best fit between the cloudy radiance from model and the observation. We use  $c^1, c^2, \dots, c^K$  to denote the array of vertical effective cloud fractions for K model levels ( $c^1$  for the surface and  $c^K$  for the model top) and  $c^0$  as the fraction of clear sky with  $0 \leq c^k \leq 1, \forall k \in [0, K]$ . The constraint for the cloud fraction is as follows,

$$\sum_{k=0}^K c^k = 1 \quad (1)$$

In this study, a cloud on one model level with a given fraction  $c^k$  is assumed to block the radiation from its lower model levels. The radiation originating from its

anna 2016-08-06 19:26 ✓  
删除的内容: effective

Administrator 2016-08-11 10:24 ✓  
带格式的: 字体颜色: 自动设置

Administrator 2016-08-08 08:35 ✓  
删除的内容: Details of the schematic of the MMR method can be referred in (Xu et al., 2015; Descombes et al., 2014).

anna 2016-08-06 20:22 ✓  
删除的内容: ,

Administrator 2016-08-11 10:24 ✓  
带格式的: 字体颜色: 自动设置

lower levels is assumed to contribute to the top of atmosphere radiance observed by the satellites only with the residual fractions.

The MMR method is an approach to retrieve cloud fractions using the minimization technique. The residual of the modeled radiance and the observation is normalized by the observed radiance, which results in the following cost function, using  $c^k$ ,  $\forall k \in [0, K]$  as the control variables,

$$J(c^0, c^1, c^2, \dots, c^K) = \frac{1}{2} \sum_v \left[ \frac{R_v^{\text{cloud}} - R_v^{\text{obs}}}{R_v^{\text{obs}}} \right]^2, \quad (2)$$

where  $R_v^{\text{cloud}}$  is the modeled cloudy radiance, and  $R_v^{\text{obs}}$  the observed radiance at frequency  $v$ . This vertical cloud fraction  $c^1, c^2, \dots, c^K$  and  $c^0$  are control variables for the cost function, where the simulated  $R_v^{\text{cloud}}$  is defined as

$$R_v^{\text{cloud}}(c^0, c^1, c^2, \dots, c^K) = c^0 R_v^0 + \sum_{k=1}^K c^k R_v^k. \quad (3)$$

Here  $R_v^k$  is the radiance calculated assuming an overcast black cloud at the model level  $k$  and  $R_v^0$  the radiance calculated in the clear sky. Both  $R_v^k$  and  $R_v^0$  are calculated using a forward radiative transfer model with model profiles of temperature and moisture as inputs. Details of the schematic of the MMR method can be referred in (Xu et al., 2015; Descombes et al., 2014).

Particle filter (PF) approach is one of the nonlinear filters for data assimilation procedures to best estimate the initial state of a system or its parameters  $x_t$ , which describes the time evolution of the full probability density function  $p(x_t)$  conditioned by the dynamics and the observations. Similar to the study in (Mechri et al., 2014), the bibliography on PF focuses on estimating the parameters, which are cloud

Administrator 2016-08-10 22:03 ✓  
 删除的内容:  $0 \leq c^k \leq 1, \forall k \in [0, K]$ .  
 anna 2016-08-06 19:54 ✓  
 删除的内容: 1

anna 2016-08-06 19:54 ✓  
 删除的内容: 2  
 anna 2016-08-06 20:00 ✓  
 删除的内容: with  $c^0 + \sum_{k=1}^K c^k = 1$  as the constraint.



fractions  $c^k$  in Eq. (3), in this study. While MMR retrieves the cloud fractions on each model vertical level by minimizing a cost function, PF calculates posterior weights for each ensemble member based on the observation likelihood given that member. In its simplest form, PF works by initializing a collection of cloud profiles as particles and then estimating the cloud distributions by averaging those particles with their corresponding weights. Each particle's weight is computed with the difference between the modeled cloudy radiance from the particle and the observed radiance.

Administrator 2016-09-10 15:20 ✓  
删除的内容: xplicitly, e

As the probabilities of the cloud distribution are fully presented by the initial particles, of particular interest is to evaluate different particle initialization schemes in the PF method. Explicitly, the definition of particles corresponds with ensemble members, i.e. one cloud profile as one of particles is corresponding to an ensemble member.

Two approaches for generating particles are firstly designed; the first one is to generate the perturbed samples  $C_b^i$  (  $\forall i \in [1, n]$  ) from the cloud profile in the background denoted as  $C_b = (c_b^0, c_b^1, \dots, c_b^K)$  by inflating (deflating) the clouds with small magnitudes (  $C_b = \alpha \times C_b, \alpha = 50\%, 55\%, \dots, 150\%$  ) and moving upward (downward) with  $\delta z = +5, +4, \dots, -1, \dots, -5$  as the vertical magnitude, where  $n$  is the sample size. The perturbed cloud fractions are designated to replenish the ensemble by introducing the prior information of the cloud distributions from the background and to increase the ensemble spread.

anna 2016-08-06 09:43 ✓  
删除的内容: typical

anna 2016-07-30 20:22 ✓  
删除的内容:  $P_b(\mathbf{c} = c^0, c^1, \dots, c^K)$   
Administrator 2016-08-08 12:54 ✓  
删除的内容: ,  
Administrator 2016-08-08 12:54 ✓  
删除的内容: , and moving

128 Besides those perturbed particles, to represent the existence of one-layer cloud

129 on each model level with an even chance, another diversity set of profiles  $C_b^i$

130 ( $\forall i \in [1, K+1]$ ) are also initialized, among which,  $C_b^i$  stands for the profile with

131 100% cloud fraction on the model level  $i$  ( $c^i=100\%$ ) and 0% cloud on the rest levels.

132 In particular,  $C_b^0$  defines 100% clear ( $c^0=1$ ). It is also interesting to discretize the

133 initial particles by setting the one-layer cloud with the value of  $c^i$  from 100% to 0%

134 (e. g., 100%, 90%, 80%, ..., 0% with 10% as the interval) and further from 100% to

135 0% (e. g., 100%, 99%, 98%, 97%, ..., 0% with 1% as the interval). In this cases,

136  $c^0=1-c^i$ . For each particle  $C_b^i$ , its simulated cloudy radiance  $R_{v,i}^{\text{cloud}}$  from the model

137 background can be obtained with Eq. (3).

138 A cost function  $J_o$  is defined for each particle to measure how the particle fit the

139 observation as,

140 
$$J_o = \frac{(R_v^{\text{obs}} - R_{v,i}^{\text{cloud}})^2}{\sigma} \quad (4)$$

141  $\sigma$  is the specified observation error, which can be referred in the first paragraph in

142 section 4.1. The weight  $w^i$  for each particle  $C_b^i$  thus is calculated by comparing

143 the simulated  $R_{v,i}^{\text{cloud}}$  and the observation  $R_v^{\text{obs}}$  using the exponential function by

144 accumulating the  $J_o$  for multiple frequency as

145 
$$w^i = e^{-\sum_v \frac{(R_v^{\text{obs}} - R_{v,i}^{\text{cloud}})^2}{\sigma}}, \quad (5)$$

146  $\forall i \in [1, n]$ . Here  $n$  is the particle size and  $\sigma$  is the specified observation error,

147 which can be referred in the first paragraph in section 4.1. The final analyzed  $C_a$  is

148 obtained by averaging the background particles  $C_b^i$  with their corresponding weight,

anna 2016-07-30 20:25 ✓

删除的内容:  $P_b$

anna 2016-07-30 20:26 ✓

删除的内容:  $P^i$

anna 2016-07-30 20:26 ✓

删除的内容:  $P^0$

anna 2016-07-30 20:26 ✓

删除的内容:  $P_b$

Administrator 2016-09-10 15:20 ✓

删除的内容: 2

anna 2016-08-06 19:17 ✓

带格式的: 缩进: 首行缩进: 0 字符

anna 2016-07-30 20:26 ✓

删除的内容:  $P_b$

anna 2016-08-06 19:15 ✓

带格式的: 字体: 倾斜

anna 2016-08-06 19:14 ✓

带格式的: 下标

anna 2016-08-06 19:55 ✓

删除的内容: 3

Administrator 2016-09-10 15:21 ✓

删除的内容:  $p$

anna 2016-08-06 19:15 ✓

删除的内容:

Administrator 2016-08-10 22:10 ✓

删除的内容:  $P$

anna 2016-07-30 20:28 ✓

删除的内容:  $P_b$

149 as

150 
$$C_a = \sum_{i=1}^p w^i C_b^i. \quad (6)$$

151 In Eq. (6), the constraint referred in Eq. (1) is not respected. Thus, after the analysis  
152 step for the particle filter, the final averaged cloud fractions  $C_a^k$  are normalized by

153 
$$C_a^k = \frac{C_a^k}{\sum_{k=0}^K C_a^k}, \quad (7)$$

154 where  $\forall k \in [0, K]$ .

### 155 3. Data and model configurations

#### 156 3.1 Data

157 The Advanced Infrared Sounder (AIRS), the Infrared Atmospheric Sounding  
158 Interferometer (IASI), and the Cross-track Infrared Sounder (CrIs) are among the  
159 most advanced hyperspectral infrared sounders and thus are applied for retrieving  
160 clouds with hundreds of channels (Blumstein et al., 2004) (Aumann et al., 2003; Xu  
161 et al., 2013; Smith et al., 2015). The Radiance measurements from Moderate  
162 Resolution Imaging Spectroradiometer (MODIS) onboard the Earth Observing  
163 System (EOS) Terra or Aqua satellites are also well suited to extracting valuable  
164 cloud information from the 36 spectral broadbands in the visible, near infrared and  
165 infrared regions at high spatial resolution (1–5 km) (Ackerman, 1998). Apart from  
166 the IR radiances from polar satellites, the Geostationary Operational Environmental  
167 Satellites (GOES) Imager (Menzel and Purdom, 1994) provides a continuous

anna 2016-08-06 19:55	✓	🔒
删除的内容: 4		
Administrator 2016-08-07 18:23	✓	🔒
删除的内容: A		
anna 2016-08-06 10:23	✓	🔒
删除的内容: updating all the particles		
anna 2016-08-06 11:17	✓	🔒
带格式的: 右		
anna 2016-08-06 11:17	✓	🔒
删除的内容:		
anna 2016-08-06 11:17	✓	🔒
删除的内容:		
anna 2016-08-06 19:55	✓	🔒
删除的内容: 5		

Administrator 2016-08-10 23:06	✓	🔒
删除的内容: (		
Administrator 2016-08-10 23:06	✓	🔒
删除的内容: )		
Administrator 2016-08-10 23:06	✓	🔒
删除的内容: (		

168 stream of data over the observing domain. In this study, GOES-13 (east) and  
169 GOES-15 (west) are also utilized to obtain cloud fractions over the continental  
170 United States (CONUS) domain. The GOES Imager used in this study is a  
171 five-channel (one visible, four infrared) imaging radiometer designed to sense  
172 radiant and solar reflected energy. The instrument parameters for the sensors and  
173 the setups for channel selections can be found in (Xu et al., 2015).

174 3.2 WRF, GSI and the radiative transfer model

175 The background fields are processed running the Weather Research and Forecast  
176 (WRF) model (Skamarock et al., 2008). The MMR and PF cloud retrieval algorithms  
177 are both implemented based on the gridpoint statistical interpolation data assimilation  
178 system (GSI) (Wu et al., 2002; Kleist et al., 2009), which is a widely used data  
179 assimilation system in operations and researches in NWP. GSI is capable of ingesting  
180 a large variety of satellite radiance observations and has developed capabilities for  
181 data thinning, quality control, and satellite radiance bias correction. The Community  
182 Radiative Transfer Model (Liu and Weng, 2006; Han et al., 2006) was used as the  
183 radiance forward operator for computing the clear-sky radiance and the radiance given  
184 overcast clouds at each model level.

185 3.3 Model configurations

186 The WRF is configured with 415\*325 horizontal grids at 15-km grid spacing,  
187 and 40 vertical levels up to 50 hPa within the single CONUS domain. The MMR and

Administrator 2016-08-10 22:59 ✓

删除的内容: (

Administrator 2016-08-10 23:00 ✓

删除的内容: (!!! INVALID CITATION !!!)

Administrator 2016-08-10 23:00 ✓

删除的内容: (

Administrator 2016-08-10 23:00 ✓

删除的内容: (!!! INVALID CITATION !!!)

PF cloud detection schemes search the cloud top using approximately 150 hPa as the highest extent for most cloudy cases. Other clouds higher 150 hPa, e.g. an anvil cloud in a mature thunderstorm around tropopause at low latitude region will also be explored in future studies. Channels in the longwave region are utilized following the channel selection scheme in (Xu et al., 2015). Since the final retrieval clouds are on model grids, the retrieved cloud fractions within one FOV are essentially extrapolated to its four neighboring model grid points. Generally, for each FOV, the retrieved cloud fractions are extrapolated to its four neighboring model grid points. For polar satellite pixels, the representative cloud fractions are extrapolated with an adaptive radius with respect to their scan positions. The cloud detecting procedure for retrieving clouds is conducted for each FOV from each individual sensor independently and sequentially. Since the clouds are retrieved FOV by FOV and the clouds on grids are referred immediately after one FOV is completed, there is no obvious accuracy loss of radiance observations using this conservative method.

Administrator 2016-08-11 10:28



带格式的: 字体颜色: 自动设置

## 4. Experiments and results

The PF experiments apply two groups of particles as mentioned in section 2, among which the group-2 particles contains solely 100% one-layer clouds. To reveal how the setup of the initial particles impacts the results, apart from the MMR and PF experiments, we included another advanced experiment, denoted as APF. APF requires more sampled particles including ranges of cloud fractions spanning from 0% to 100% at the interval of 10%. An additional experiment “APFg2”, similar to APF

but excluding the perturbed particles from the background in group-1 introduced in section 2, was conducted to evaluate the added values from the group-one particles. In this section, cloud retrieval experiments for several cases containing clouds of a variety of types are conducted for comparison reason. The GOES imager retrieved products from National Aeronautics and Space Administration (NASA-Langley cloud and radiation products) are applied as a reference to validate the cloud retrieving methods for the CONUS domain with a large and uniform coverage of cloud mask. In addition, the retrieved cloud products were also compared to available CloudSat (Stephens et al., 2002) and MODIS level-2 cloud products (Platnick et al., 2003) archived by the CloudSat Data Processing Center in Colorado State and NASA respectively.

#### 4.1 Single test at one field of view

The PF cloud retrieving algorithm retrieves the cloud distributions by averaging those initial particles with their weights. Before the real case experiments are carried out over the whole domain, we conduct a single cloud retrieving test at one FOV to understand what differences can be explained by the differences in the basic initial particles. In Eq. (5), the observation error  $\sigma$  can be set proportional to the

observation, equaling to  $\frac{R_v^{\text{obs}}}{r}$ , where  $r$  is the prescribed ratio. Thus, the cloud

signals on each level  $k$  are virtually determined by the extent of how close the  $\frac{R_v^k}{R_v^{\text{obs}}}$

(and  $\frac{R_v^0}{R_v^{\text{obs}}}$  for the clear part) gets to 1. An example of the ratio of the overcast

anna 2016-08-06 19:55



删除的内容: 7

radiance and the observed radiance  $\frac{R_v^k}{R_v^{obs}}$  for each model level is given in Fig. 1 of  
 GOES-Imager for the channel 5 ( $\sim 13.00 \mu m$ ). The clear sky radiance normalized by  
 the observed radiance  $\frac{R_v^0}{R_v^{obs}}$  is also shown at the level 0 (Fig. 1). It is expected that  
 the overcast radiance from the RTM decrease with the rising of the altitude. The  
 cloud signal is strongest around level 5, where  $R_v^k$  fits  $R_v^{obs}$  most closely. The  
 cloud retrievals depend not only on the basic input profiles (i.e., the overcast  
 radiance on each level from RTM normalized by the observed radiance and the clear  
 sky radiance from RTM normalized by the observed radiance) and but also on the  
 algorithm applied for resolving the problem (e.g., MMR and PF in this study).

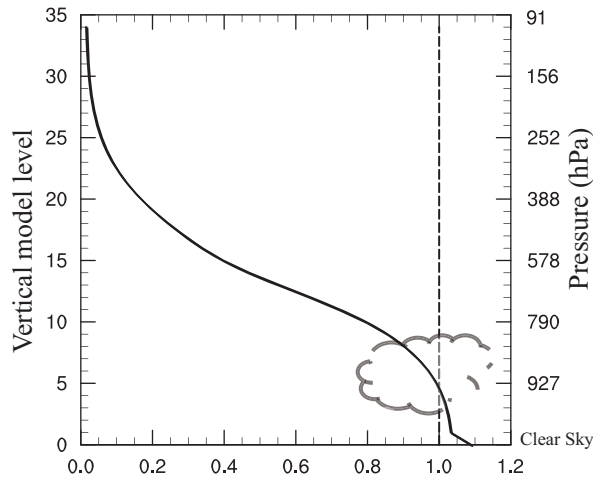


**Figure 1.** Ratio of the overcast radiances versus the observed radiance starting from the level 1.  
 The ratio of the clear sky radiance normalized by the observed radiance corresponds to the level  
 0 (see text for explanation) for GOES-Imager for the channel 5. The approximate pressures  
 corresponding to the model levels are also denoted.

244 To reveal the roles of various initial particles, Fig. 2a shows the weights for  
 245 different particles on the given FOV for channel 5 of GOES-Imager for the case  
 246 shown in Fig. 1. Particles in Fig. 1 include one-layer cloud in group 2 described in  
 247 section 2 with specified value of cloud fractions  $c^k$  (on the x-axis) on specified  
 248 model levels  $k$  (on the y-axis) from 10% to 100% every 10%. With a fraction  $c^k$  of  
 249 one-cloud layer at a given level  $k$  and a fraction of  $c^0 = 1 - c^k$  of clear sky, the  
 250 simulated cloudy radiance can be denoted as  $R_v^{\text{cloud}} = c^k R_v^k + (1 - c^k) R_v^0$ . Hence the  
 251 theoretical one-layer cloud fraction is solved as  $c^k = \frac{R_v^0 - R_v^{\text{obs}}}{R_v^0 - R_v^k}$  by fitting  $R_v^{\text{cloud}}$  to  
 252  $R_v^0$ . As expected, for one-layer cloud with full fraction,  $c^5$  equals to 100%. Since  
 253 with the concept that  $R_v^k > R_v^{k+1}$ , no cloud can be present below level 5 since this  
 254 would implies a  $R_v^{\text{cloud}}$  larger than the observation (or a  $c^i$  larger than 100%). It  
 255 seems that clouds can be described by different possible states as particles with both  
 256 large fractions and small fractions. Low clouds are easily estimated by one-layer  
 257 cloud profile with large fractions (larger than 10%). The particles with small-fraction  
 258 high clouds gain some weights to retrieve high clouds. The particle with the  
 259 one-layer cloud on level 13 seems to gain least weight compared to the others levels.  
 260 The weights for the particles with cloud fractions from 0% to 100% at the interval of  
 261 1% are also presented in Fig. 2b. By including more small-fraction one-layer clouds,  
 262 the clouds around level 13 can be reproduced by the group of refined particles with  
 263 1% as the interval for approximate 10% cloud fractions. However, changing the  
 264 level of the cloud for the fixed fraction (10%) does not seem to change the outgoing  
 265 radiance much, probably due to the channel's low weight function peak (~750hPa).

Administrator 2016-08-22 17:02	✓	🔒
删除的内容: of		
Administrator 2016-09-10 15:24	✓	🔒
删除的内容: of		
Administrator 2016-08-08 11:06	✓	🔒
带格式的: 字体: 倾斜		
Administrator 2016-09-10 15:25	✓	🔒
删除的内容: on the given FOV for channel 5 of GOES-Imager for the case shown in Fig. 1		
Administrator 2016-08-11 10:35	✓	🔒
带格式的: 字体颜色: 自动设置		

Administrator 2016-08-11 10:35	✓	🔒
带格式的: 字体颜色: 自动设置		
Administrator 2016-08-08 11:13	✓	🔒
删除的内容: by		



The normalized  $J_o$  in Eq. (6) for different levels with a specific cloud fraction from 0% to 100% every 10% are shown in the bottom panel of Fig. 3, with 10% and 1% as the intervals in Fig. 3c and Fig. 3d respectively. Here,  $J_o$  can be further derived as

$$J_o = r^2 \left( 1 - c^0 \frac{R_v^0}{R_v^{obs}} - c^k \frac{R_v^k}{R_v^{obs}} \right)^2$$

(8), with  $\sigma = \frac{R_v^{obs}}{r}$  and  $R_v^{cloud}(c^0, c^1, c^2, \dots, c^K) = c^0 R_v^0 + \sum_{k=1}^K c^k R_v^k$ .

From Fig. 3a, it is found that  $J_o$  is smallest around level-5 with 100% cloud fraction (denoted as 1 in legend) for the thin black line, with respect to the fact that the overcast radiance fits the observed radiance most closely for level-5 approximately. The grey line with 10% cloud fraction (0.1 in the legend) corresponds to the existence of a weight peak on level 19 in Fig. 2a. In addition, the gap between the grey line with 0.1 and the other lines from 0.2 to 1 explains why there's less continuity around level 13. Fig. 3b shows a similar pattern to Fig. 3a, except with densely-distributed  $J_o$  values around the level 13 from 0.1 to 1 in the legend. Those contiguous black lines in Fig. 3b are associated with the set of particles with cloud fractions from 10% to 100% at the interval of 1%.

Administrator 2016-09-10 15:25	✓	🔒
删除的内容: 2		
Administrator 2016-09-10 15:25	✓	🔒
删除的内容: 2		
Administrator 2016-09-10 15:25	✓	🔒
删除的内容: 2		

Administrator 2016-08-11 13:50	✓	🔒
删除的内容:		
Administrator 2016-09-10 15:25	✓	🔒
删除的内容: 2		
Administrator 2016-09-10 15:25	✓	🔒
删除的内容: c		

Administrator 2016-09-10 15:26	✓	🔒
删除的内容: 2d		
Administrator 2016-09-10 15:26	✓	🔒
删除的内容: 2c,		
Administrator 2016-09-10 15:26	✓	🔒
删除的内容: 2d		

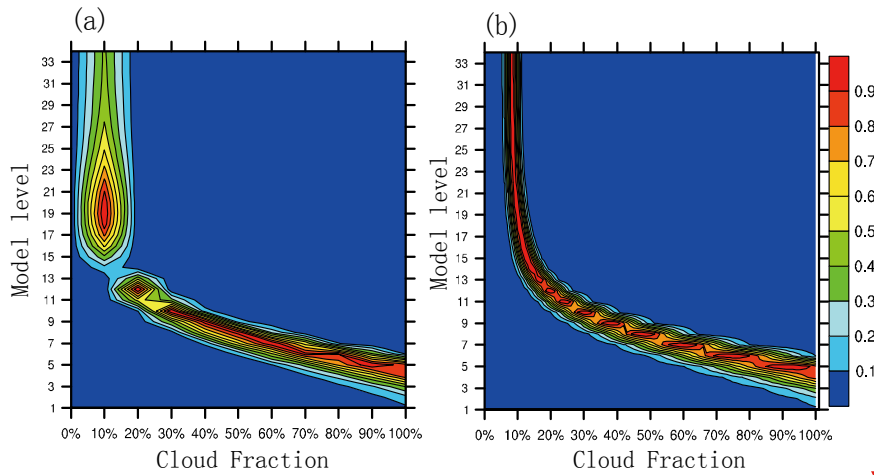


**Figure 2.** The weights for different particles with specified cloud fractions on the x-axis at one chosen model level shown on the y-axis from 0% to 100% (a) at the interval of 10% and (b) at the interval of 1%.

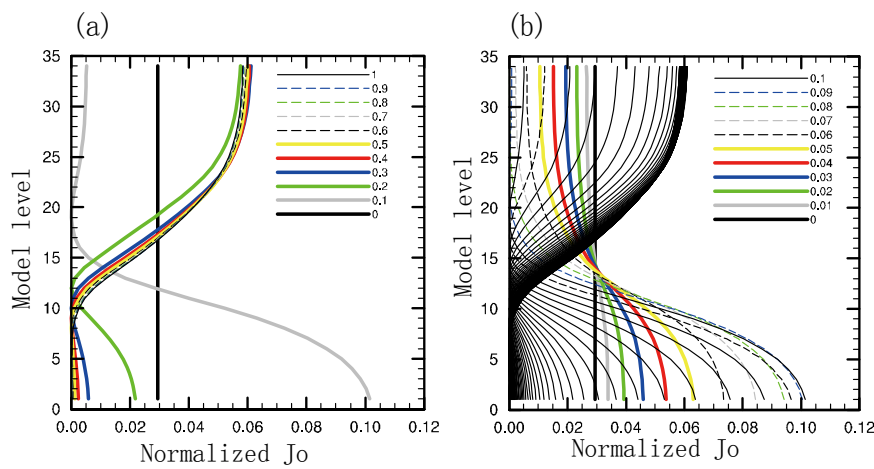
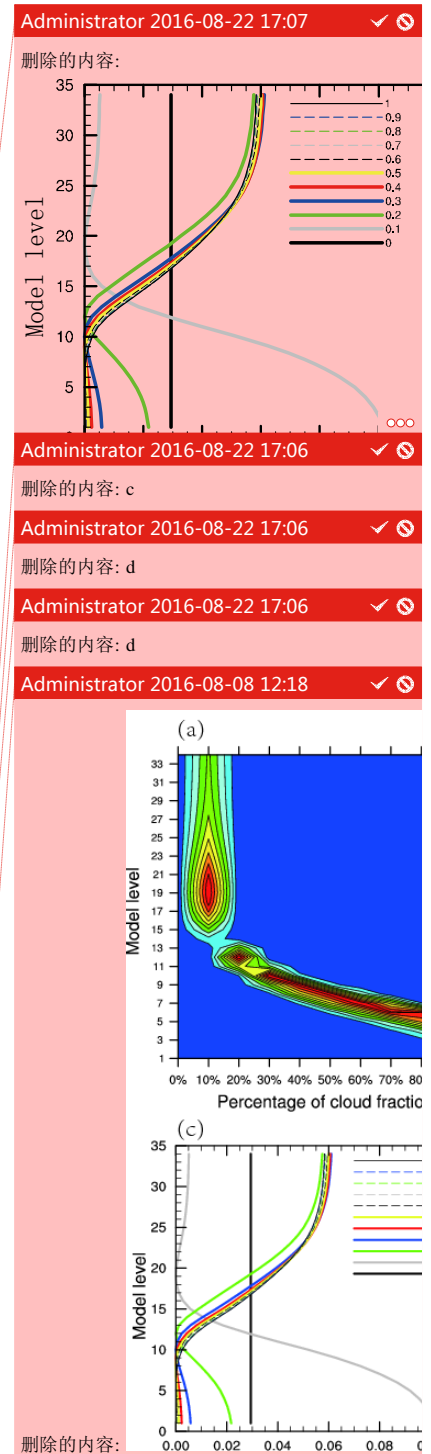


**Figure 3.** The normalized  $J_o$  (a) at the interval of 10% and (b) at the interval of 1%. In (b), the normalized  $J_o$  from 0.1 to 1 are all denoted as black lines.



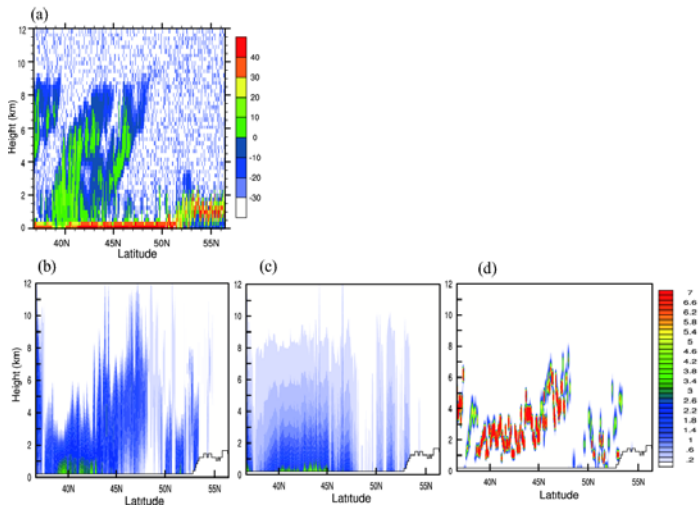
291 4.2 Cloud profiles

292 The retrieval experiments for a real case are conducted at 1100 UTC 3 June 2012  
293 when AIRS measurements and the CloudSat “2B-GEOPROF” products (Mace, 2004)  
294 are available. The vertical cross sections of the cloud fraction field of a real case are  
295 illustrated to further check how different collections of initial particles impact the  
296 retrieved cloud profiles. The standard radar reflectivity profiles from the CloudSat  
297 are shown in Fig. 4a as the validation source; Fig. 4b, Fig. 4c, and Fig. 4d show the  
298 cross sections of the cloud fractions along the CloudSat orbit tracks from the MMR,  
299 PF and APF experiments. The vertical structures of the clouds from MMR compare  
300 well with the radar reflectivity from CloudSat by retrieving the high clouds around  
301 47N° and low clouds around 52N°. The PF experiment has difficulties in detecting  
302 the cloud tops appropriately. PF tends to detect a large quantity of low clouds; by  
303 adding a set of particles with small-fraction clouds in APF, higher clouds can be  
304 reproduced, which is consistent with the implications from Fig. 2b and 3b. APF  
305 detects clear strong cloud signals and removes the cloud fractions on near-surface  
306 levels around 36 N° successfully. Since the existences of ground-layer radar  
307 reflectivity are likely corresponding to the strong reflection from the underlying  
308 surface of the earth, the height of cloud bases of MMR and PF are not compared in  
309 this sub-section. The experiments with larger size of particles including 0% to 20%  
310 (at the interval of 1%) plus 30% to 100% (at the interval of 10%) or of 0% to 100%  
311 (at the interval of 1%) one-layer cloud profiles (introduced in section 2) yield similar  
312 results from APF but are much more costly (not shown).

Administrator 2016-09-10 15:27 ✓  
删除的内容: Figure 2. The weights for different particles with specified cloud fractions on the x-axis at one chosen model level shown on the y-axis from 0% to 100% (a) at the interval of 10% and (b) at the interval of 1%. The normalized  $J_o$  (c) at the interval of 10% and (d) at the interval of 1%. In (d), the normalized  $J_o$  from 0.1 to 1 are all denoted as black lines.

Administrator 2016-09-10 15:28 ✓  
删除的内容: 3  
Administrator 2016-09-10 15:28 ✓  
删除的内容: 3  
Administrator 2016-09-10 15:28 ✓  
删除的内容: 3  
Administrator 2016-09-10 15:28 ✓  
删除的内容: 3

Administrator 2016-09-10 15:28 ✓  
删除的内容: 2d



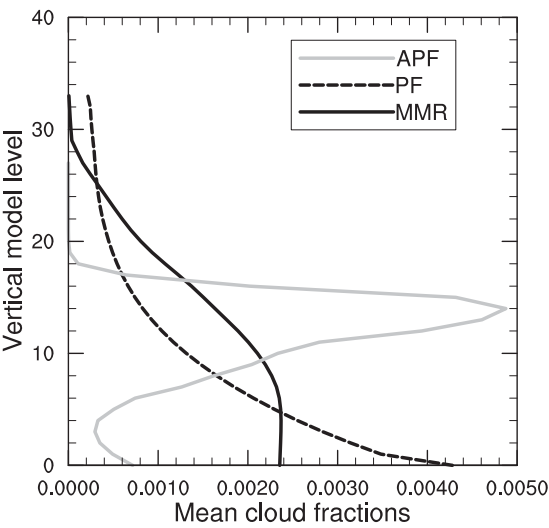
314

315 **Figure 4.** (a) The radar reflectivity (units: DBZ) cross sections from CloudSat, (b) the MMR  
316 retrieved cloud fractions (units: %) cross sections, (c) the PF retrieved cloud fractions, and (d)  
317 the APF retrieved cloud fractions valid at 1100 UTC 3 June 2012.

318 The vertical profiles of the averaged cloud fractions from MMR, PF, and APF are  
319 plotted in Fig. 5 at 1100 UTC 3 June 2012 with AIRS. Both MMR and PF  
320 experiments yield ambiguous cloud distributions, whereas APF retrieves much  
321 stronger cloud signals constrained between level-2 to level-20 (approximately from  
322 950hPa to 400hPa). More clouds around level 10 are retrieved (approximately  
323 750hPa) in MMR, while PF is prone to retrieving clouds near surface levels. Note  
324 that MMR retrieves much higher cloud tops and lower cloud bases compared to APF.  
325 The cloud base from PF is lowest; the cloud top from MMR and PF is comparable.  
326 Only the APF related methods will be further discussed in later sections owing to the  
327 missing of high clouds using PF.

Administrator 2016-09-10 15:28 ✓  
删除的内容: 3

Administrator 2016-09-10 15:28 ✓  
删除的内容: 4



329

330 **Figure 5.** The mean cloud fraction on all model levels for the experiments MMR, PF, and APF  
331 [with AIRS observations](#) valid at 1100 UTC 3 June 2012.

332 4.3 Cloud mask

333 Comparison experiments on real cases are further performed for over longer time  
334 period from 0000 UTC 12 December 2013 to 0700 UTC 12 December 2013. The  
335 cloud mask is marked as cloudy when there is a recognizable existence of cloud on  
336 any level from MMR or PF retrievals. Both the NASA GOES Imager products and the  
337 MMR-retrieved fields are interpolated to the same  $0.1^{\circ}\times0.1^{\circ}$  latitude–longitude grid  
338 with 0 for clear and 1 for cloudy before the comparisons for verification. Fig. 6 shows  
339 the *hits*, *false\_alarms* and *misses* locations with the use of [GOES-Imager](#), MODIS,  
340 CrIS, AIRS, and IASI [radiances](#) in the retrieval algorithms at 0700 UTC 12 December  
341 2013. Note that, cloud mask retrievals from both the MMR and APF hit the clear and  
342 cloudy events well in Fig. 6a and 6b. In most areas, the MMR experiment

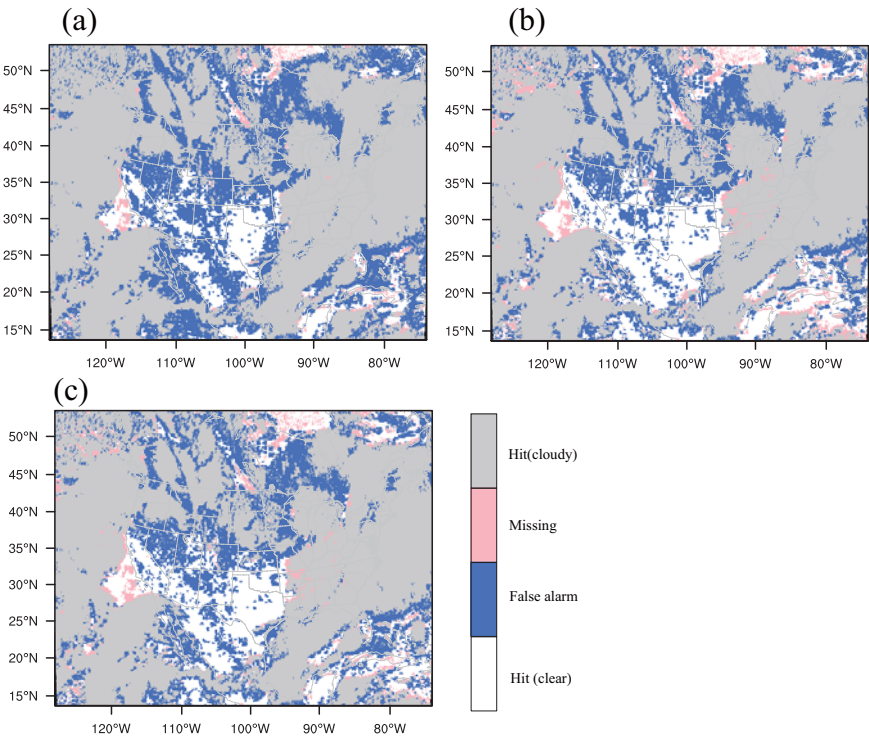
Administrator 2016-09-10 15:29	✓	🔒
删除的内容: 4		
anna 2016-08-06 08:35	✓	🔒
删除的内容: from		

Administrator 2016-09-10 15:29	✓	🔒
删除的内容: 5		
anna 2016-08-06 08:39	✓	🔒
删除的内容: radiances from		
Administrator 2016-09-10 15:29	✓	🔒
删除的内容: 5		
Administrator 2016-09-10 15:29	✓	🔒
删除的内容: 5		

343 overestimated the cloud mask with more false alarm events compared to the APF  
344 experiment, since the MMR solution is an “overly smoothed” estimation of the true  
345 vertical profile. It seems that the accuracy of cloud detection is lower for areas with  
346 high altitude than under tropical conditions, indicating that the smaller lapse rate in  
347 the atmosphere will lead radiance less sensitivity to clouds over polar areas. Fig. 6c  
348 shows the cloud mask results from the APFg2 experiment without the perturbed  
349 particles in group-1 introduced in section 2. There is no large discrepancy between  
350 Fig. 6b and Fig. 6c, suggesting that the particles in group-2 that fully span the  
351 possibility of the cloud distributions, are more determinant in retrieving the cloud  
352 mask.  
353

Administrator 2016-09-10 15:29 ✓  
删除的内容: 5

Administrator 2016-09-10 15:30 ✓  
删除的内容: 5  
Administrator 2016-09-10 15:30 ✓  
删除的内容: 5



355 **Figure 6.** The false alarms, misses, and hits for clear and cloudy event locations with (a) the  
356 MMR method, (b) the APF method, and (c) the APF method but without the group-1 particles  
357 (see text for detailed explanations) valid at 0700 UTC 15 December 2013.

Administrator 2016-09-10 15:30 ✓  
删除的内容: 5

358 4.4 Cloud top and base pressure

359 The retrieved cloud top pressures (CTP) and cloud bottom pressures (CBP) from  
360 this study along with the NASA GOES cloud products are illustrated in Fig. 7. The  
361 CTPs from both methods are in good accordance with the NASA cloud products for  
362 high clouds (from 100 hPa to 600 hPa) in Fig. 7a, 7c, and 7e. The retrieved cloud top  
363 heights from MMR are overall higher than those from the NASA reference, especially  
364 for lower clouds at approximately 750-1000 hPa (e. g., between longitude -100° and  
365 -90°). On the other hand, the CTPs from APF are much closer to those in the  
366 reference for both high and low clouds. APF overestimates the CBPs for some low  
367 clouds (putting the clouds too low) in Fig. 7f; the overestimation of the CBP is even  
368 more obvious from MMR in most regions in Fig. 7d.

Administrator 2016-09-10 15:31 ✓  
删除的内容: 6

Administrator 2016-09-10 15:31 ✓  
删除的内容: 6

Administrator 2016-09-10 15:31 ✓  
删除的内容: 6

Administrator 2016-09-10 15:31 ✓  
删除的内容: 6

Administrator 2016-09-10 15:31 ✓  
删除的内容: 6

Administrator 2016-09-10 15:31 ✓  
删除的内容: 6



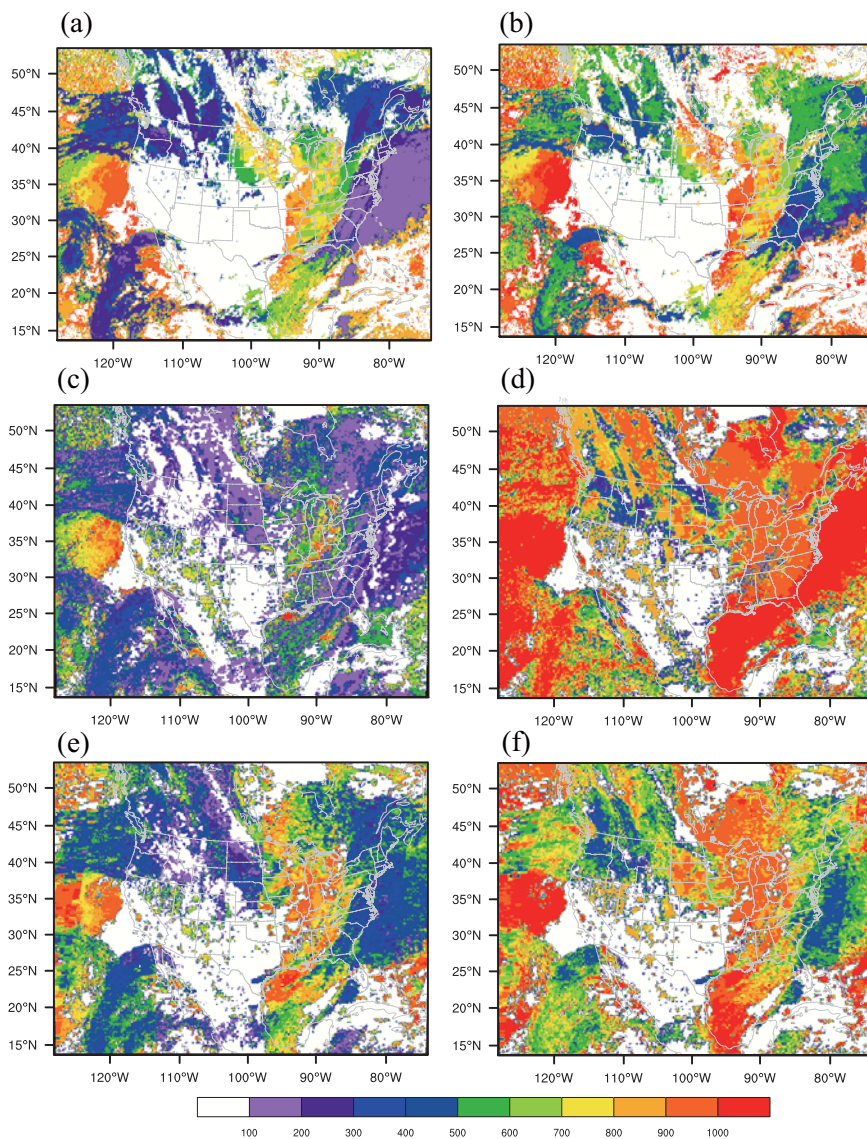


**Figure 7.** The cloud top pressure (left panels) from (a) the NASA GOES retrieval, (c) the MMR method, (e) the APF method, and the cloud bottom pressure (right panels) from (b) the NASA GOES retrieval, (d) the MMR method, (f) the APF method valid at 0700 UTC 15 December 2013.

The CTPs from NASA GOES cloud products for more hours (0300UTC, 0500UTC, 0700UTC) together with the independent CTP retrievals from MODIS

Administrator 2016-09-10 15:32



删除的内容: 6



level-2 products ([http://modis-atmos.gsfc.nasa.gov/MOD06\\_L2/](http://modis-atmos.gsfc.nasa.gov/MOD06_L2/)) are plotted in Fig. 8. Different sub-periods of the MODIS cloud retrieval products (e.g., Fig. 8b valid at 0320 UTC, Fig. 8c at 0325, and Fig. 8d at 0330 UTC) are chosen to approach the valid times in Fig. 8a, Fig. 8e, and Fig. 8h respectively. The CTPs from both cloud products agree well for both high and low clouds, confirming that NASA GOES cloud products are overall reliable for verifying the cloud retrievals and MODIS level-2 products can also be applied for validations.

[illegible]

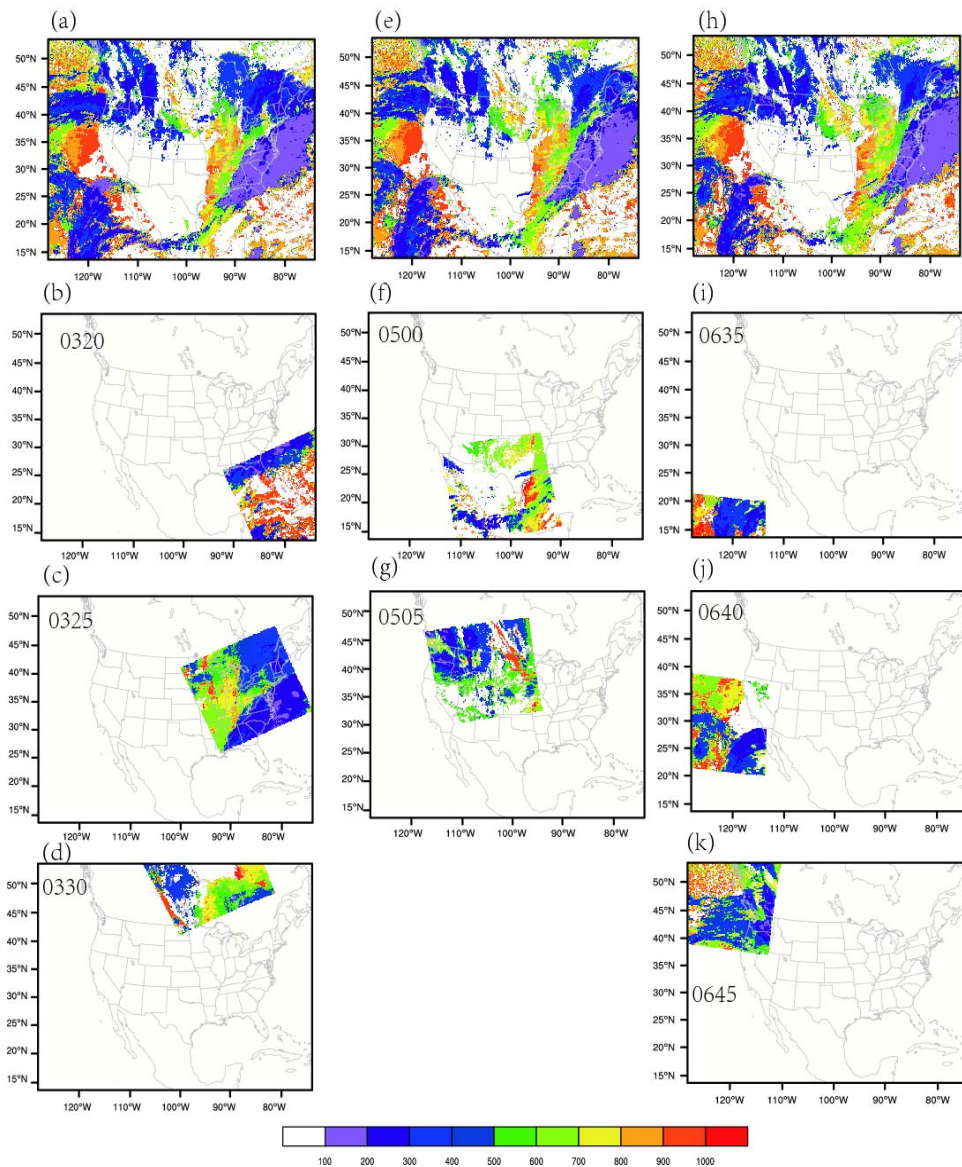


**Figure 8.** The cloud top pressure for (a) 0300UTC from the GOES NASA retrieval, (b) 0320UTC, (c) 0325UTC, (d) 0330UTC from MODIS level-2 products; (e) 0500UTC from the GOES NASA retrieval, (f) 0500UTC, (g) 0505UTC; (h) 0700UTC from the GOES NASA retrieval, (i) 0635UTC, (j) 0640UTC, and (k) 0645UTC from MODIS level-2 products.

Administrator 2016-09-10 15:33



删除的内容: 7

Fig. 9 presents the correlation coefficients and biases of the CTP and CBP verified against the NASA GOES and MODIS retrievals. The solid lines denote the results regarding the CTP and CBP versus the NASA GOES products from 0000 UTC to 0700 UTC, while the dots describe the CTP results versus the cloud top retrievals in NASA MODIS level-2 products at 0320UTC, 0325UTC, 0330UTC, 0500UTC, 0505UTC, 0635UTC, 0640UTC, and 0645UTC. Here the negative bias means that the retrieved clouds are higher than the reference. Vice versa, the positive bias indicates the clouds are put too low. We conducted another experiment “APFimg” that applies solely GOES Imager data to check the added value from the high spectral resolution radiances (such as, CrIS, AIRS, and IASI). In Fig. 9a, the correlations between the retrievals from MMR and the NASA GOES retrievals are comparable with from APF for most hours; APF gains overall higher correlations with the CTPs in the MODIS retrievals. From the bias in Fig. 9b, it seems that the CTPs from MMR are underestimated (putting the clouds too high) consistently against both retrievals with GOES and MODIS radiances. Fig. 9c shows that the correlations are weaker for MMR compared to others all the time. In Fig. 9d, the positive CBP biases from MMR are remarkable, while the CBP biases from APF are largely reduced. Generally, APFimg degrades the CTP and CBP results consistently, suggesting that radiances with high spectral resolutions are able to improve the vertical descriptions of cloud profiles. It is found that the clouds retrieved with APFg2 are shrunken in terms of cloud depth with notably lower cloud top and higher cloud base compared to APF, when excluding the perturbed particles in the first

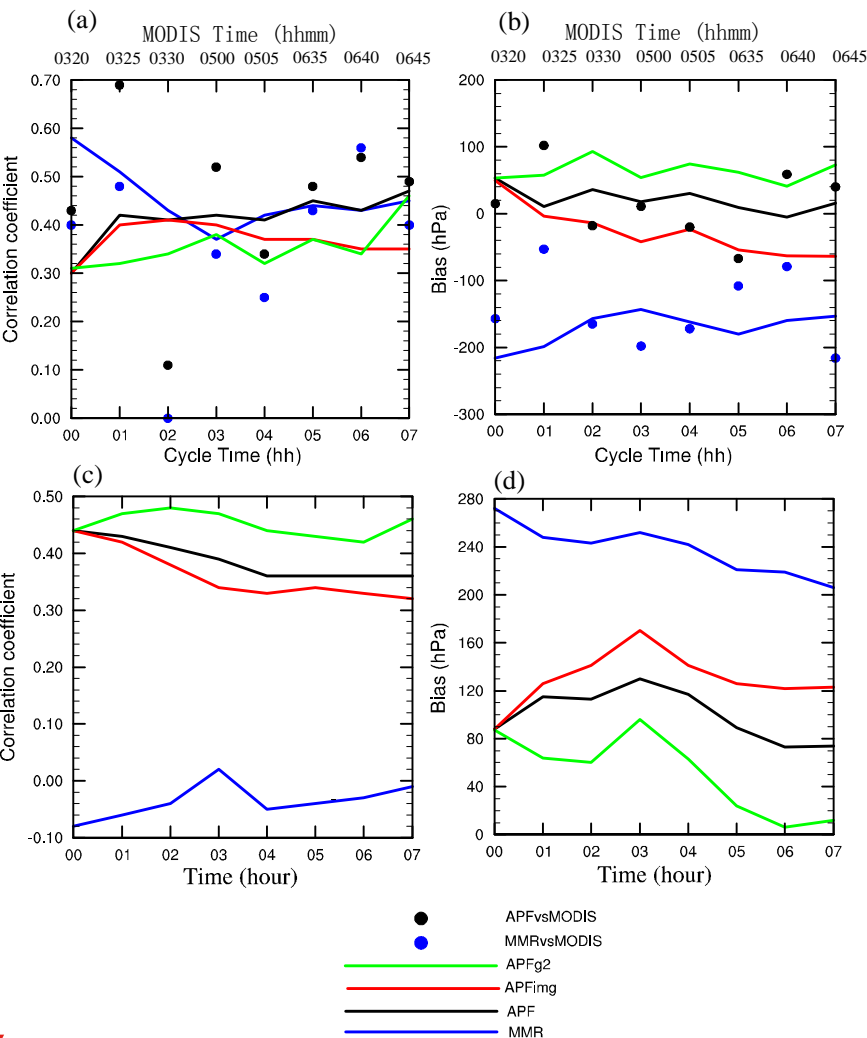
Administrator 2016-09-10 15:33 ✓  
删除的内容: 8

Administrator 2016-09-10 15:33 ✓  
删除的内容: 8

Administrator 2016-09-10 15:33 ✓  
删除的内容: 8

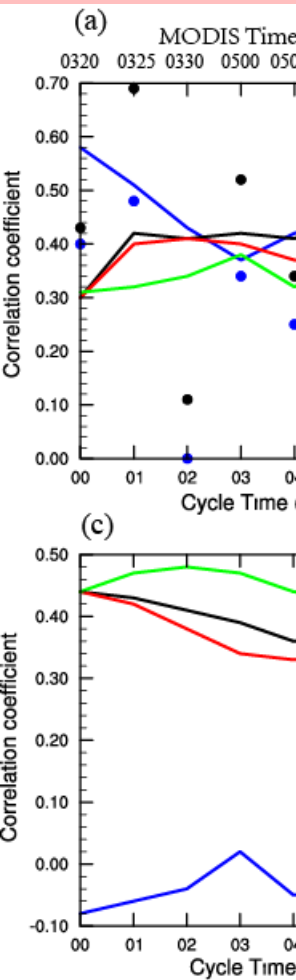
anna 2016-08-06 08:40 ✓  
删除的内容: from  
Administrator 2016-09-10 15:33 ✓  
删除的内容: 8  
Administrator 2016-09-10 15:34 ✓  
删除的内容: 8

410 group.



411  
412 **Figure 2.** (a) Correlation coefficient, (b) bias for the cloud top pressure, (c) correlation  
413 coefficient, and (d) bias for the cloud bottom pressure versus the NASA GOES retrievals from  
414 0600 UTC 15 December 2013 to 0700 UTC 15 December 2013. Black and blue dots denote  
415 results versus the MODIS level-2 cloud top pressure retrieval valid at 0320UTC, 0325UTC,  
416 0330UTC, 0500UTC, 0505UTC, 0635UTC, 0640UTC, and 0645UTC. The valid times for the

Administrator 2016-08-08 12:20 ✓



删除的内容:

Administrator 2016-09-10 15:34 ✓

删除的内容: 8

417 MODIS level-2 data are shown on the top of the x-axis.

418 4.5 Computational issues

419 Fig. 10a represents the elapsed times for the MMR and APF experiments and the  
420 counts of radiance observations in use are shown in Fig. 10b from 0000 UTC to  
421 0700 UTC 12 December 2013. The profile of computing time in MMR is quite  
422 different from that in PF. The cost of MMR is dominated by the heavy minimization  
423 procedure, while APF is more associated with the processes of initializing particles  
424 and calculating weights for all the particles. The computing times were measured  
425 from cloud retrieving runs with 64 MPI-tasks on a single computing node in an IBM  
426 iDataPlex Cluster. The measured wall clock computing times show that generally  
427 MMR is computationally more expensive for most of the time than APF. It seems  
428 the wall clock times for MMR are generally proportional to the data amount used.  
429 While for the APF experiment, the wall clock time is mostly determined by the  
430 particles size and partly affected by the channel number, such as for 2013121202 and  
431 2013121206, when the total counts of the hyperspectral sensors (IASI, CrIs, and  
432 AIRS) are large. The PF experiments using particles of one-layer cloud with 100%  
433 cloud fractions usually take less than 5 minutes for the same periods (not shown).

Administrator 2016-09-10 15:34 ✓

删除的内容: 9

Administrator 2016-09-10 15:34 ✓

删除的内容: 9

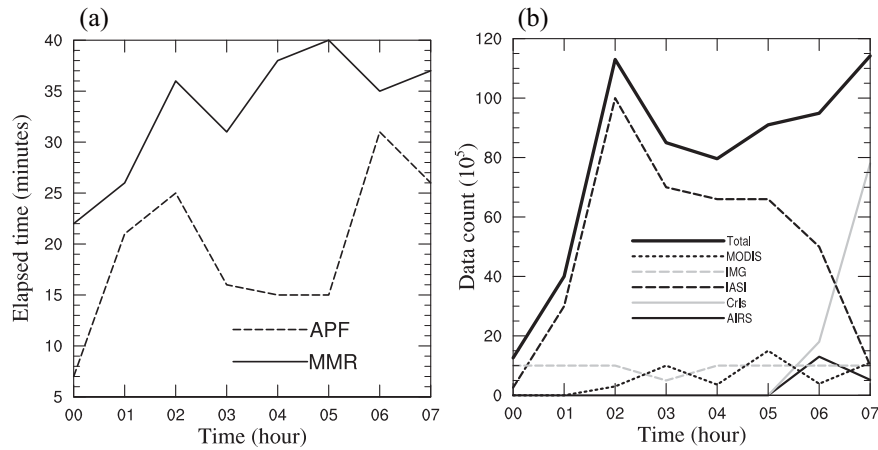


**Figure 10.** (a) The elapsed time and (b) the data count from 0000 UTC to 0700 UTC 15

December 2013.

Administrator 2016-09-10 15:34

删除的内容: 9

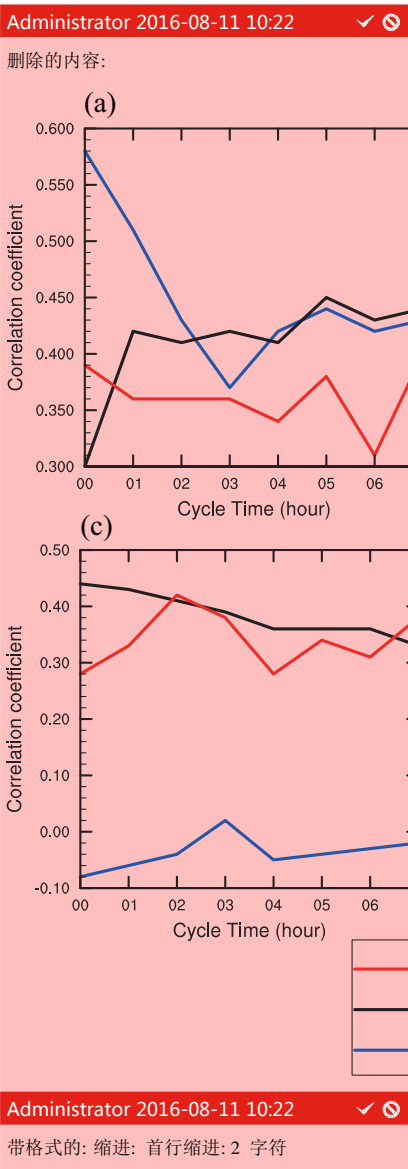
#### 4.6 Resolving the filtering problem on model grids

As explained in subsection 3.3, the filtering problem is resolved in the radiance observational space at each FOV of each sensor independently and sequentially. For each FOV, the retrieved cloud fractions are extrapolated to its neighboring model grid points afterwards. We order the sensors in the cloud retrieving procedure as GOES-Imager, MODIS, CrIS, AIRS, and IASI, aiming to optimize the vertical clouds using sensors featured with sufficient spectral resolutions. As a consequence, the retrievals from the last sensor determine the final output to the most extent, causing the cloud retrievals highly subjective to the ordering of the sensors. On the other hand, it means the information from other prior sensors will be more or less discarded. In this section, a different way of resolving the filtering problem is preliminarily tested, in which the weights for each particle are aggregated over all

449 available sensors by calling the forward radiative transfer model on neighbouring  
450 model grids.

451 Fig. 1 shows the clouds retrievals from the grid-based method. It is noted that  
452 the grid-based scheme yields slightly worse results of CTP and neutral results of  
453 CBP compared with those from the observation-based (FOV-based) scheme,  
454 indicating that the hyperspectral sensors probably favor the retrieved CTP and CBP  
455 in the FOV-based scheme, which are available for most of the time. It is worth  
456 pointing out that the ordering of different sensors has nearly no effect on the final  
457 cloud retrievals, when the weights of the particles are calculated in model space (not  
458 shown). The final cloud retrieval is no longer overwritten by the retrieval from the  
459 last sensor but is a total solution with all the sensors fairly considered, instead. The  
460 computational cost of retrieving clouds in model space is comparable or slightly  
461 heavier than that in observation space. The computational cost of the grid-based  
462 scheme scales with the number of the computing nodes more directly, compared to  
463 that of the FOV-based scheme.

Administrator 2016-09-10 15:34 ✓  
删除的内容: 0



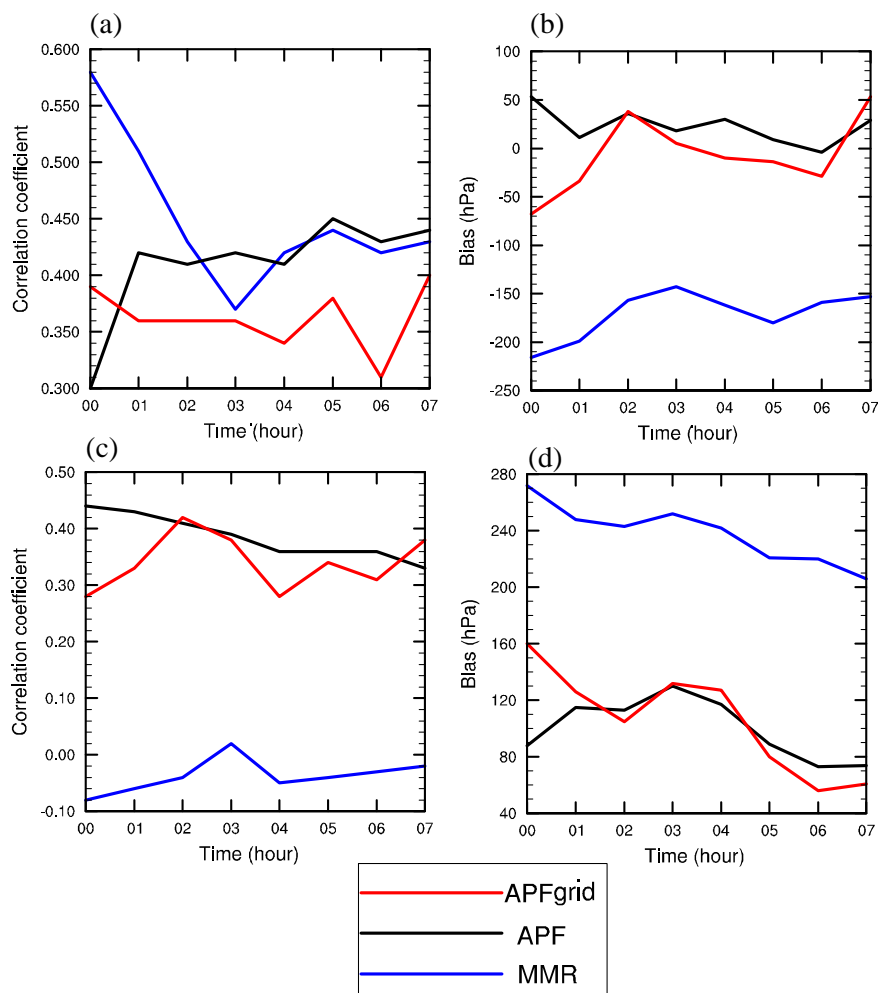


**Figure 11.** (a) Correlation coefficient, (b) bias for the cloud top pressure, (c) correlation coefficient, and (d) bias for the cloud bottom pressure versus the NASA GOES retrievals from 0000 UTC to 0700 UTC 15 December 2013.

## 5. Discussion and conclusion

Administrator 2016-09-10 15:34

删除的内容: 0



469        This study presents a new cloud retrieval method based on the particle filter (PF)  
470        in the framework of GSI, as a competitive alternative to the MMR method. The  
471        behaviors of different particle initializations are demonstrated on one single field of  
472        view and the CONUS domain respectively. Comparisons between the PF and the  
473        MMR method are conducted in terms of the features of cloud mask, cloud top, cloud  
474        base, and the vertical distributions of clouds. It was found that the PF method  
475        retrieves clear cloud signals while MMR is more ambiguous in detecting clouds. By  
476        adding more small-fraction particles, high clouds can be better interpreted. From the  
477        statistical results, it was found that MMR underestimates the cloud top pressures (put  
478        the clouds top too high) and overestimates the cloud bottom pressures (put the  
479        clouds top too low) as well. APF improves both the retrievals of cloud tops and  
480        cloud bases remarkably, especially for the cloud bases. As expected, radiances with  
481        high spectral resolutions contribute to quantitative cloud top and cloud base  
482        retrievals. In addition, a different way of resolving the filtering problem over each  
483        model grid is tested to aggregate the weights with all available sensors considered,  
484        which is proven to be less constrained by the ordering of sensors. Last but not least,  
485        the PF method is overall more computationally efficient; the cost of the model  
486        grid-based PF method scales more directly with the number of the computing nodes.

487        In future work, validation studies using multispectral imagers on geostationary  
488        satellites, spaceborne lidars (or radar), and surface site data will continue, and the  
489        results will be used to update the retrieval algorithm. Maximizing the consistency in  
490        the products across platforms and optimizing the synergistic use of multiple-source

491 radiances in the new algorithm are important aspects. To estimate the flow dependent  
492 uncertainties in the cloud analysis and in the forecasts, the ensemble nowcasting with  
493 three dimensional cloud fractions via the rapid-update cycling mode is also planned.  
494 [Increasing the highest extent cloudy cases will be included in future studies.](#) Finally,  
495 the use of cloud liquid water and ice mixing ratios retrieved from the cloud fractions  
496 using multi-sensor radiances to pre-process the first guess in numerical weather  
497 forecast is another promising application.

#### 498 **Code and/or data availability**

499 The MMR cloud retrieval codes can be obtained freely from  
500 (<http://www2.mmm.ucar.edu/wrf/users/wrfda/>). The other codes can be obtained by  
501 emails from the authors.

#### 502 **Acknowledgments**

503 This work was jointly sponsored by the the US Air Force Weather Agency under the  
504 project "Air Force Coupled Analysis and Prediction System", Natural Science  
505 Foundation of Jiangsu Province under Grant No BK20160954, the 973 Program  
506 (Grant No. 2013CB430102), the Beijige Funding from Jiangsu Research Institute of  
507 Meteorological Science (BJG201510), the National Natural Science Foundation of  
508 China (41375025), and the Priority Academic Program Development of Jiangsu  
509 Higher Education Institutions (PAPD). The authors would like to thank Chris Davis  
510 for fruitful discussions, and to Bobbie Weaver for editing the manuscript. We greatly  
511 thank the anonymous reviewers for their valuable comments on the earlier versions of  
512 the manuscript.

## REFERENCES

- Ackerman, S. A., K. I. Strabala, W. P. Menzel, R. A. Frey, C. C. Moeller, and L. E. Gumley: Discriminating clear sky from clouds with MODIS, *Geophys. Res. Atmos.*, 103, 32141-32157, 1998.
- Auligné, T., Lorenc, A., Michel, Y., Montmerle, T., Jones, A., Hu, M., and Dudhia, J.: Toward a New Cloud Analysis and Prediction System, *B Am Meteorol Soc*, 92, 207-210, 2011.
- Auligné, T.: Multivariate minimum residual method for cloud retrieval. Part I: Theoretical aspects and simulated observation experiments, *Monthly Weather Review*, 142, 4383-4398, 2014a.
- Auligné, T.: Multivariate minimum residual method for cloud retrieval. Part II: Real observations experiments, *Monthly Weather Review*, 142, 4399-4415, 2014b.
- Aumann, H. H., Chahine, M. T., Gautier, C., Goldberg, M. D., Kalnay, E., McMillin, L. M., Revercomb, H., Rosenkranz, P. W., Smith, W. L., and Staelin, D. H.: AIRS/AMSU/HSB on the Aqua mission: Design, science objectives, data products, and processing systems, *Geoscience and Remote Sensing, IEEE Transactions on*, 41, 253-264, 2003.
- Bayler, G. M., Aune, R., and Raymond, W.: NWP cloud initialization using GOES sounder data and improved modeling of nonprecipitating clouds, *Monthly weather review*, 128, 3911-3920, 2000.
- Berrocal, V. J., Raftery, A. E., and Gneiting, T.: Combining spatial statistical and ensemble information in probabilistic weather forecasts, *Monthly Weather Review*, 135, 1386-1402, 2007.
- Blumstein, D., Chalon, G., Carlier, T., Buil, C., Hebert, P., Maciaszek, T., Ponce, G., Phulpin, T., Tournier, B., and Simeoni, D.: IASI instrument: Technical overview and measured performances, *Optical Science and Technology, the SPIE 49th Annual Meeting*, 2004, 196-207,
- Brückner, M., Pospichal, B., Macke, A., and Wendisch, M.: A new multispectral cloud retrieval method for ship - based solar transmissivity measurements, *Journal of Geophysical Research: Atmospheres*, 119, 2014.
- Descombes, G., Auligne, T., and Lin, H.-C., Xu, D., Schwartz, C. S., Vandenberghe, F.: Multi-sensor Advection Diffusion nowCast (MADCast) for cloud analysis and short-term prediction., *NCAR Technical Note NCAR/TN-509+STR*, , 21 pp., 2014.
- Eyre, J. R., and Menzel, W. P.: Retrieval of cloud parameters from satellite sounder data: A simulation study, *Journal of Applied Meteorology*, 28, 267-275, 1989.
- Han, Y., Delst, P. V., Liu, Q., Weng, F., Yan, B., Treadon, R., and Derber, J.: JCSDA Community Radiative Transfer Model (CRTM)—Version 1, *NOAA Tech. Rep. NESDIS*, 122, 33, 2006.
- Hu, M., Xue, M., and Brewster, K.: 3DVAR and Cloud Analysis with WSR-88D Level-II Data for the Prediction of the Fort Worth, Texas, Tornadoic Thunderstorms. Part I: Cloud Analysis and Its Impact, *Monthly Weather Review*, 134, 675-698, 10.1175/mwr3092.1, 2006.

Huang, H.-L., Smith, W. L., Li, J., Antonelli, P., Wu, X., Knuteson, R. O., Huang, B., and Osborne, B. J.: Minimum local emissivity variance retrieval of cloud altitude and effective spectral emissivity-simulation and initial verification, *Journal of applied meteorology*, 43, 795-809, 2004.

Karlsson, K.-G., Johansson, E., and Devasthale, A.: Advancing the uncertainty characterisation of cloud masking in passive satellite imagery: Probabilistic formulations for NOAA AVHRR data, *Remote Sensing of Environment*, 158, 126-139, 2015.

Kleist, D. T., Parrish, D. F., Derber, J. C., Treadon, R., Wu, W. S., and Lord, S.: Introduction of the GSI into the NCEP Global Data Assimilation System, *Weather and Forecasting*, 24, 1691-1705, 10.1175/2009waf2222201.1, 2009.

Liu, Q., and Weng, F.: Advanced doubling-adding method for radiative transfer in planetary atmospheres, *Journal of the atmospheric sciences*, 63, 3459-3465, 2006.

Mace, G. G., 2004: Level 2 GEOPROF product process description and interface control document (v.3): Level 2 GEOPROF product process description and interface control document (v.3), Tech. rep., CIRA, Colorado State University, 2004.

Mechri, R., Ottlé, C., Pannekoucke, O., and Kallel, A.: Genetic particle filter application to land surface temperature downscaling, *Journal of Geophysical Research: Atmospheres*, 119, 2131-2146, 2014.

Menzel, W., Smith, W., and Stewart, T.: Improved cloud motion wind vector and altitude assignment using VAS, *Journal of Climate and Applied meteorology*, 22, 377-384, 1983.

Menzel, W. P., and Purdom, J. F.: Introducing GOES-I: The first of a new generation of geostationary operational environmental satellites, *B Am Meteorol Soc*, 75, 757-781, 1994.

Platnick, S., King, M. D., Ackerman, S. A., Menzel, W. P., Baum, B. A., Riédi, J. C., and Frey, R. A.: The MODIS cloud products: Algorithms and examples from Terra, *Geoscience and Remote Sensing, IEEE Transactions on*, 41, 459-473, 2003.

Rossow, W. B., and Schiffer, R. A.: ISCCP cloud data products, *B Am Meteorol Soc*, 72, 2-20, 1991.

Rossow, W. B., Walker, A. W., and Garder, L. C.: Comparison of ISCCP and other cloud amounts, *Journal of Climate*, 6, 2394-2418, 1993.

Shen, Z. Q., and Tang, Y. M.: A modified ensemble Kalman particle filter for non-Gaussian systems with nonlinear measurement functions, *J Adv Model Earth Sy*, 7, 50-66, 2015.

Skamarock, W., C, Klemp, J. B., Dudhia, J., Gill, D. O., Barker, D. M., Duda, G., Huang, X.-Y., Wang, W., and Powers, J. G.: A description of the Advanced Research WRF version 3., NCAR, 113, 2008.

Smith, A., Atkinson, N., Bell, W., and Doherty, A.: An initial assessment of observations from the Suomi - NPP satellite: data from the Cross - track Infrared Sounder (CrIS), *Atmospheric Science Letters*, 16, 260-266, 2015.

- Snyder, C., and Zhang, F. Q.: Assimilation of simulated Doppler radar observations with an ensemble Kalman filter, *Monthly Weather Review*, 131, 1663-1677, Doi 10.1175//2555.1, 2003.
- Stephens, G. L., Vane, D. G., Boain, R. J., Mace, G. G., Sassen, K., Wang, Z., Illingworth, A. J., O'Connor, E. J., Rossow, W. B., and Durden, S. L.: The CloudSat mission and the A-Train: A new dimension of space-based observations of clouds and precipitation, *B Am Meteorol Soc*, 83, 1771-1790, 2002.
- van Leeuwen, P. J.: Nonlinear data assimilation in geosciences: an extremely efficient particle filter, *Quarterly Journal of the Royal Meteorological Society*, 136, 1991-1999, 2010.
- Wu, W.-S., Purser, R. J., and Parrish, D. F.: Three-dimensional variational analysis with spatially inhomogeneous covariances, *Monthly Weather Review*, 130, 2905-2916, 2002.
- Wu, X., and Smith, W. L.: Assimilation of ERBE data with a nonlinear programming technique to improve cloud-cover diagnostics, 120, 2009-2004, 1992.
- Xu, D., Auligné, T., and Huang, X.-Y.: A Retrieval Method for 3-D Cloud Parameters Using Radiance Observations from Multiple Satellites, *Advances in atmospheric physics*, 32, 349-362, 2015.
- Xu, D. M., Liu, Z. Q., Huang, X. Y., Min, J. Z., and Wang, H. L.: Impact of assimilating IASI radiance observations on forecasts of two tropical cyclones, *Meteorology and Atmospheric Physics*, 122, 1-18, 10.1007/s00703-013-0276-2, 2013.
- Zhao, C., Xie, S., Klein, S. A., Protat, A., Shupe, M. D., McFarlane, S. A., Comstock, J. M., Delanoë, J., Deng, M., and Dunn, M.: Toward understanding of differences in current cloud retrievals of ARM ground - based measurements, *Journal of Geophysical Research: Atmospheres*, 117, 2012.

A method for retrieving clouds with satellite infrared  
radiances using the particle filter

Dongmei Xu<sup>1,2</sup>, Thomas Auligné<sup>2</sup>, Gaël Descombes<sup>2</sup>, and Chris Snyder<sup>2</sup>

<sup>1</sup>[Key Laboratory of Meteorological Disaster, Ministry of Education \(KLME\) /Joint International Research Laboratory of Climate and Environment Change \(ILCEC\) /Collaborative Innovation Center on Forecast and Evaluation of Meteorological Disasters \(CIC-FEMD\), Nanjing University of Information Science & Technology, Nanjing 210044, China](#)

<sup>2</sup>National Center for Atmospheric Research, Boulder, Colorado 80301, USA

(2016/9/10)

Administrator	2016-08-08 10:37	✓	🔒
带格式的: 法语(法国)			
Administrator	2016-09-10 15:00	✓	🔒
删除的内容: y			
Administrator	2016-08-08 10:37	✓	🔒
带格式的: 法语(法国)			

anna	2016-07-30 20:16	✓	🔒
删除的内容: Collaborative Innovation Center on Forecast and Evaluation of Meteorological Disasters, Nanjing University of Information Science & Technology, Nanjing, 210044, China			
Administrator	2016-09-10 15:16	✓	🔒
删除的内容: 78			
anna	2016-08-11 07:21	✓	🔒
删除的内容: 30			
Administrator	2016-09-10 15:16	✓	🔒
删除的内容: 1			

\* Corresponding Author

Dr. Dongmei Xu

Nanjing University of Information Science & Technology, College of Atmospheric science,  
Ningliu road, No. 219, Nanjing, 210044, China

E-mail: [xdmjolly@sina.com](mailto:xdmjolly@sina.com)

## Abstract

Ensemble-based techniques have been widely utilized in estimating uncertainties in various problems of interest in geophysical applications. A new cloud retrieval method is proposed based on the Particle Filter (PF) [by using ensembles of cloud information](#) in the framework of Gridpoint Statistical Interpolation system (GSI). The PF cloud retrieval method is compared with the Multivariate and Minimum Residual (MMR) method that was previously established and verified. Cloud retrieval experiments involving a variety of cloudy types are conducted with the PF and MMR methods respectively with measurements of Infrared radiances on multi-sensors onboard both geostationary and polar satellites. It is found that the retrieved cloud masks with both methods are consistent with other independent cloud products. MMR is prone to producing ambiguous small-fraction clouds, while PF detects clearer cloud signals, yielding closer heights of cloud top and cloud base to other references. More collections of small fraction particles are able to effectively estimate the semi-transparent high clouds. It is found that radiances with high spectral resolutions contribute to quantitative cloud top and cloud base retrievals. In addition, a different way of resolving the filtering problem over each model grid is tested to better aggregate the weights with all available sensors considered, which is proven to be less constrained by the ordering of sensors. Compared to the MMR method, the PF method is overall more computationally efficient, and the cost of the model grid-based PF method scales more directly with the number of computing nodes.

Keywords: cloud retrieval methods, particle filter, GSI system, cloud height

Administrator 2016-09-10 15:17 ✓

删除的内容: efficient

## 1. Introduction

Modern polar orbiting and geostationary airborne instruments provide researchers unprecedented opportunities for remote sensing of earth with continuous flows and almost complete spectral coverage of data. The primary cloud retrieval products from satellites are cloud mask (CM), cloud height (CH), effective cloud fraction (CF), and vertical structures of clouds with larger temporal and spatial scales. These cloud retrievals provide an immense and valuable combination for better initializing hydrometeors in numerical weather prediction (NWP), (Wu and Smith, 1992; Hu et al., 2006; Bayler et al., 2000; Auligné et al., 2011) regulating the radiation budget for the planet, and understanding the climate feedback mechanism (Rossow and Schiffer, 1991; Rossow et al., 1993; Brückner et al., 2014). Advanced cloud retrieval methods are able to retrieve clouds with multispectral techniques (Menzel et al., 1983; Platnick et al., 2003), among which the minimization methods usually directly utilize the difference between the modeled clear sky and the observed cloudy Infrared (IR) radiances i.e. g., the minimum residual method, (Eyre and Menzel, 1989); the Minimum Local Emissivity Variance method, (Huang et al., 2004); and the Multivariate Minimum Residual method, (Auligné, 2014a). Specially, the Multivariate Minimum Residual (MMR) method is retrieving three dimensional multi-layer clouds by minimizing a cost function at each field-of-view (FOV) (Auligné, 2014b; Xu et al., 2015). MMR has been proven to be reliable in retrieving the quantitative three dimensional cloud fractions with Infrared radiances from

Administrator 2016-09-10 15:17



删除的内容: earth

Administrator 2016-09-10 15:18



删除的内容: (

Administrator 2016-09-10 15:18



删除的内容: )



58 multiple infrared instruments. However, MMR has limitations in several aspects due  
59 to its use of minimization for solution: 1) Part of the control variables accounting for  
60 the cloud fraction for some certain levels are under-observed since the channels are  
61 not sensitive to the existence of clouds for those heights. 2) When clouds at different  
62 heights show opacities with the same spectral signal, MMR could lose the ability to  
63 distinguish solutions involving clouds at those levels. 3) The computational cost for  
64 the minimization procedure in MMR is rather considerable.

65 Ensemble-based techniques, that usually reside in short-term ensemble  
66 forecasting (Berrocal et al., 2007), assembling existing model outputs (e. g., cloud  
67 retrievals) from varying algorithms (Zhao et al., 2012), or ensemble Kalman filter  
68 (EnKF) in diversified forms (Snyder and Zhang, 2003), have been widely developed  
69 in order to estimate the uncertainties of various problems in geophysical applications.

70 To better account for the non-linearity between the observed radiance and the retrieval  
71 parameter, a novel prototype for detecting clouds and retrieving their vertical  
72 extension inspired by the particle filter (Snyder and Zhang, 2003; van Leeuwen, 2010;  
73 Shen and Tang, 2015) technique and Bayesian theory (Karlsson et al., 2015) is  
74 proposed in this study. As a competitive alternative for MMR, the PF retrieval method  
75 has same critical inputs required and cloud retrieval products as in MMR. A brief  
76 description of MMR and the new PF cloud retrieval algorithm are provided in the  
77 following section. Section 3 describes the background model, the data assimilation  
78 system, the radiative transfer models (RTMs), and the radiance observations applied  
79 in this study. Model configurations are also illustrated in section 3. In section 4, the

Administrator 2016-09-10 15:18	✓	🔒
删除的内容: various		
Administrator 2016-09-10 15:19	✓	🔒
删除的内容: all kinds of		

single test within one FOV is conducted before the performance of PF method is assessed by comparing its cloud retrievals with those from MMR and other operational cloud products. Section 4 also discusses the computational performance for the two methods. The conclusion and anticipated future work are outlined in section 5.

## 2. Methodology

Essentially, the PF cloud retrieval scheme retrieves clouds with the same critical inputs requested (i. e., clear sky radiance from the radiative transfer model and the observed radiance) and the same cloud retrievals as outputs (i. e., three dimensional cloud fractions, which is defined as the fraction of top of cloud as seen from a sensor) with the MMR method. Both cloud retrieval schemes consist of finding cloud fractions that allow best fit between the cloudy radiance from model and the observation. We use  $c^1, c^2, \dots, c^K$  to denote the array of vertical effective cloud fractions for K model levels ( $c^1$  for the surface and  $c^K$  for the model top) and  $c^0$  as the fraction of clear sky with  $0 \leq c^k \leq 1, \forall k \in [0, K]$ . The constraint for the cloud fraction is as follows,

$$\sum_{k=0}^K c^k = 1 \quad (1)$$

In this study, a cloud on one model level with a given fraction  $c^k$  is assumed to block the radiation from its lower model levels. The radiation originating from its

anna 2016-08-06 19:26 ✓  
删除的内容: effective

Administrator 2016-08-11 10:24 ✓  
带格式的: 字体颜色: 自动设置

Administrator 2016-08-08 08:35 ✓  
删除的内容: Details of the schematic of the MMR method can be referred in (Xu et al., 2015; Descombes et al., 2014).

anna 2016-08-06 20:22 ✓  
删除的内容: ,

Administrator 2016-08-11 10:24 ✓  
带格式的: 字体颜色: 自动设置

99 lower levels is assumed to contribute to the top of atmosphere radiance observed by  
100 the satellites only with the residual fractions.

101 The MMR method is an approach to retrieve cloud fractions using the  
102 minimization technique. The residual of the modeled radiance and the observation is  
103 normalized by the observed radiance, which results in the following cost function,  
104 using  $c^k, \forall k \in [0, K]$  as the control variables,

$$105 \quad J(c^0, c^1, c^2, \dots, c^K) = \frac{1}{2} \sum_v \left[ \frac{R_v^{\text{cloud}} - R_v^{\text{obs}}}{R_v^{\text{obs}}} \right]^2, \quad (2)$$

106 where  $R_v^{\text{cloud}}$  is the modeled cloudy radiance, and  $R_v^{\text{obs}}$  the observed radiance at  
107 frequency  $v$ . This vertical cloud fraction  $c^1, c^2, \dots, c^K$  and  $c^0$  are control variables for  
108 the cost function, where the simulated  $R_v^{\text{cloud}}$  is defined as

$$109 \quad R_v^{\text{cloud}}(c^0, c^1, c^2, \dots, c^K) = c^0 R_v^0 + \sum_{k=1}^K c^k R_v^k. \quad (3)$$

110 Here  $R_v^k$  is the radiance calculated assuming an overcast black cloud at the model  
111 level  $k$  and  $R_v^0$  the radiance calculated in the clear sky. Both  $R_v^k$  and  $R_v^0$  are  
112 calculated using a forward radiative transfer model with model profiles of temperature  
113 and moisture as inputs. Details of the schematic of the MMR method can be referred  
114 in (Xu et al., 2015; Descombes et al., 2014).

115 Particle filter (PF) approach is one of the nonlinear filters for data assimilation  
116 procedures to best estimate the initial state of a system or its parameters  $x_t$ , which  
117 describes the time evolution of the full probability density function  $p(x_t)$  conditioned  
118 by the dynamics and the observations. Similar to the study in (Mechri et al., 2014), the  
119 bibliography on PF focuses on estimating the parameters, which are cloud fractions

Administrator 2016-08-10 22:03 ✓  
删除的内容:  $0 \leq c^k \leq 1, \forall k \in [0, K]$ .  
anna 2016-08-06 19:54 ✓  
删除的内容: 1

anna 2016-08-06 19:54 ✓  
删除的内容: 2  
anna 2016-08-06 20:00 ✓  
删除的内容: with  $c^0 + \sum_{k=1}^K c^k = 1$  as the constraint.

$c^k$  in Eq. (3), in this study. While MMR retrieves the cloud fractions on each model vertical level by minimizing a cost function, PF calculates posterior weights for each ensemble member based on the observation likelihood given that member. In its simplest form, PF works by initializing a collection of cloud profiles as particles and then estimating the cloud distributions by averaging those particles with their corresponding weights. Each particle's weight is computed with the difference between the modeled cloudy radiance from the particle and the observed radiance.

Administrator 2016-09-10 15:20 ✓  
删除的内容: xplicitly, e

As the probabilities of the cloud distribution are fully presented by the initial particles, of particular interest is to evaluate different particle initialization schemes in the PF method. Explicitly, the definition of particles corresponds with ensemble members, i.e. one cloud profile as one of particles is corresponding to an ensemble member.

Two approaches for generating particles are firstly designed; the first one is to generate the perturbed samples  $C_b^i$  (  $\forall i \in [1, n]$  ) from the cloud profile in the background denoted as  $C_b = (c_b^0, c_b^1, \dots, c_b^K)$  by inflating (deflating) the clouds with small magnitudes (  $C_b = \alpha \times C_b, \alpha = 50\%, 55\%, \dots, 150\%$  ) and moving upward (downward) with  $\delta z = +5, +4, \dots, -1, \dots, -5$  as the vertical magnitude, where  $n$  is the sample size. The perturbed cloud fractions are designated to replenish the ensemble by introducing the prior information of the cloud distributions from the background and to increase the ensemble spread.

anna 2016-08-06 09:43 ✓  
删除的内容: typical

anna 2016-07-30 20:22 ✓  
删除的内容:  $P_b(\mathbf{c} = c^0, c^1, \dots, c^K)$   
Administrator 2016-08-08 12:54 ✓  
删除的内容: ,  
Administrator 2016-08-08 12:54 ✓  
删除的内容: , and moving

Besides those perturbed particles, to represent the existence of one-layer cloud on each model level with an even chance, another diversity set of profiles  $C_b^i$

anna 2016-07-30 20:25 ✓  
删除的内容:  $P_b^i$

142 (  $\forall i \in [1, K+1]$  ) are also initialized, among which,  $C_b^i$  stands for the profile with  
 143 100% cloud fraction on the model level  $i$  ( $c^i=100\%$ ) and 0% cloud on the rest levels.

144 In particular,  $C_b^0$  defines 100% clear ( $c^0=1$ ). It is also interesting to discretize the  
 145 initial particles by setting the one-layer cloud with the value of  $c^i$  from 100% to 0% (e.

146 g., 100%, 90%, 80%, ..., 0% with 10% as the interval) and further from 100% to 0%  
 147 (e. g., 100%, 99%, 98%, 97%, ..., 0% with 1% as the interval). In this cases,  $c^0=1-c^i$ .

148 For each particle  $C_b^i$ , its simulated cloudy radiance  $R_{v,i}^{\text{cloud}}$  from the model background  
 149 can be obtained with Eq. (3).

150 A cost function  $J_o$  is defined for each particle to measure how the particle fit the  
 151 observation as,

$$J_o = \left( \frac{R_v^{\text{obs}} - R_{v,i}^{\text{cloud}}}{\sigma} \right)^2. \quad (4)$$

153  $\sigma$  is the specified observation error, which can be referred in the first paragraph in  
 154 section 4.1. The weight  $w^i$  for each particle  $C_b^i$  thus is calculated by comparing the  
 155 simulated  $R_{v,i}^{\text{cloud}}$  and the observation  $R_v^{\text{obs}}$  using the exponential function by  
 156 accumulating the  $J_o$  for multiple frequency as

$$w^i = e^{-\sum_v \left( \frac{R_v^{\text{obs}} - R_{v,i}^{\text{cloud}}}{\sigma} \right)^2}, \quad (5)$$

158  $\forall i \in [1, n]$ . Here  $n$  is the particle size and  $\sigma$  is the specified observation error,  
 159 which can be referred in the first paragraph in section 4.1. The final analyzed  $C_a$  is  
 160 obtained by averaging the background particles  $C_b^i$  with their corresponding weight,  
 161 as

$$C_a = \sum_{i=1}^p w^i C_b^i. \quad (6)$$

anna 2016-07-30 20:26 ✓  
 删除的内容: P<sup>i</sup>

anna 2016-07-30 20:26 ✓  
 删除的内容: P<sup>0</sup>

anna 2016-07-30 20:26 ✓  
 删除的内容: P<sub>b</sub>

Administrator 2016-09-10 15:20 ✓  
 删除的内容: 2

anna 2016-08-06 19:17 ✓  
 带格式的: 缩进: 首行缩进: 0 字符

anna 2016-07-30 20:26 ✓  
 删除的内容: P<sub>b</sub>

anna 2016-08-06 19:15 ✓  
 带格式的: 字体: 倾斜

anna 2016-08-06 19:14 ✓  
 带格式的: 下标

anna 2016-08-06 19:55 ✓  
 删除的内容: 3

Administrator 2016-09-10 15:21 ✓  
 删除的内容: p

anna 2016-08-06 19:15 ✓  
 删除的内容:

Administrator 2016-08-10 22:10 ✓  
 删除的内容: P

anna 2016-07-30 20:28 ✓  
 删除的内容: P<sub>b</sub>

anna 2016-08-06 19:55 ✓  
 删除的内容: 4

In Eq. (6), the constraint referred in Eq. (1) is not respected. Thus, after the analysis step for the particle filter, the final averaged cloud fractions  $c_a^k$  are normalized by

$$c_a^k = \frac{c^k}{\sum_{k=0}^K c^k}, \quad (7)$$

where  $\forall k \in [0, K]$ .

### 3. Data and model configurations

#### 3.1 Data

The Advanced Infrared Sounder (AIRS), the Infrared Atmospheric Sounding Interferometer (IASI), and the Cross-track Infrared Sounder (CrIs) are among the most advanced hyperspectral infrared sounders and thus are applied for retrieving clouds with hundreds of channels (Blumstein et al., 2004) (Aumann et al., 2003; Xu et al., 2013; Smith et al., 2015). The Radiance measurements from Moderate Resolution Imaging Spectroradiometer (MODIS) onboard the Earth Observing System (EOS) Terra or Aqua satellites are also well suited to extracting valuable cloud information from the 36 spectral broadbands in the visible, near infrared and infrared regions at high spatial resolution (1–5 km) (Ackerman, 1998). Apart from the IR radiances from polar satellites, the Geostationary Operational Environmental Satellites (GOES) Imager (Menzel and Purdom, 1994) provides a continuous stream of data over the observing domain. In this study, GOES-13 (east) and GOES-15 (west) are also utilized to obtain cloud fractions over the continental United States

Administrator 2016-08-07 18:23	✓	🔒
删除的内容: A		
anna 2016-08-06 10:23	✓	🔒
删除的内容: updating all the particles		
anna 2016-08-06 11:17	✓	🔒
带格式的: 右		
anna 2016-08-06 11:17	✓	🔒
删除的内容:		
anna 2016-08-06 11:17	✓	🔒
删除的内容:		
anna 2016-08-06 19:55	✓	🔒
删除的内容: 5		

Administrator 2016-08-10 23:06	✓	🔒
删除的内容: (		
Administrator 2016-08-10 23:06	✓	🔒
删除的内容: )		
Administrator 2016-08-10 23:06	✓	🔒
删除的内容: (		

182 (CONUS) domain. The GOES Imager used in this study is a five-channel (one  
183 visible, four infrared) imaging radiometer designed to sense radiant and solar  
184 reflected energy. The instrument parameters for the sensors and the setups for  
185 channel selections can be found in (Xu et al., 2015).

186 3.2 WRF, GSI and the radiative transfer model

187 The background fields are processed running the Weather Research and Forecast  
188 (WRF) model (Skamarock et al., 2008). The MMR and PF cloud retrieval algorithms  
189 are both implemented based on the gridpoint statistical interpolation data assimilation  
190 system (GSI) (Wu et al., 2002; Kleist et al., 2009), which is a widely used data  
191 assimilation system in operations and researches in NWP. GSI is capable of ingesting  
192 a large variety of satellite radiance observations and has developed capabilities for  
193 data thinning, quality control, and satellite radiance bias correction. The Community  
194 Radiative Transfer Model (Liu and Weng, 2006; Han et al., 2006) was used as the  
195 radiance forward operator for computing the clear-sky radiance and the radiance given  
196 overcast clouds at each model level.

197 3.3 Model configurations

198 The WRF is configured with 415\*325 horizontal grids at 15-km grid spacing, and  
199 40 vertical levels up to 50 hPa within the single CONUS domain. The MMR and PF  
200 cloud detection schemes search the cloud top using approximately 150 hPa as the  
201 highest extent for most cloudy cases. Other clouds higher 150 hPa, e.g. an anvil cloud

Administrator 2016-08-10 22:59 ✓

删除的内容: (

Administrator 2016-08-10 23:00 ✓

删除的内容: (!!! INVALID CITATION !!!)

Administrator 2016-08-10 23:00 ✓

删除的内容: (

Administrator 2016-08-10 23:00 ✓

删除的内容: (!!! INVALID CITATION !!!)

in a mature thunderstorm around tropopause at low latitude region will also be explored in future studies. Channels in the longwave region are utilized following the channel selection scheme in (Xu et al., 2015). Since the final retrieval clouds are on model grids, the retrieved cloud fractions within one FOV are essentially extrapolated to its four neighboring model grid points. Generally, for each FOV, the retrieved cloud fractions are extrapolated to its four neighboring model grid points. For polar satellite pixels, the representative cloud fractions are extrapolated with an adaptive radius with respect to their scan positions. The cloud detecting procedure for retrieving clouds is conducted for each FOV from each individual sensor independently and sequentially. Since the clouds are retrieved FOV by FOV and the clouds on grids are referred immediately after one FOV is completed, there is no obvious accuracy loss of radiance observations using this conservative method.

Administrator 2016-08-11 10:28



带格式的: 字体颜色: 自动设置

## 4. Experiments and results

The PF experiments apply two groups of particles as mentioned in section 2, among which the group-2 particles contains solely 100% one-layer clouds. To reveal how the setup of the initial particles impacts the results, apart from the MMR and PF experiments, we included another advanced experiment, denoted as APF. APF requires more sampled particles including ranges of cloud fractions spanning from 0% to 100% at the interval of 10%. An additional experiment “APFg2”, similar to APF but excluding the perturbed particles from the background in group-1 introduced in section 2, was conducted to evaluate the added values from the group-one particles. In



this section, cloud retrieval experiments for several cases containing clouds of a variety of types are conducted for comparison reason. The GOES imager retrieved products from National Aeronautics and Space Administration (NASA-Langley cloud and radiation products) are applied as a reference to validate the cloud retrieving methods for the CONUS domain with a large and uniform coverage of cloud mask. In addition, the retrieved cloud products were also compared to available CloudSat (Stephens et al., 2002) and MODIS level-2 cloud products (Platnick et al., 2003) archived by the CloudSat Data Processing Center in Colorado State and NASA respectively.

#### 4.1 Single test at one field of view

The PF cloud retrieving algorithm retrieves the cloud distributions by averaging those initial particles with their weights. Before the real case experiments are carried out over the whole domain, we conduct a single cloud retrieving test at one FOV to understand what differences can be explained by the differences in the basic initial particles. In Eq. (5), the observation error  $\sigma$  can be set proportional to the

observation, equaling to  $\frac{R_v^{\text{obs}}}{r}$ , where  $r$  is the prescribed ratio. Thus, the cloud

signals on each level  $k$  are virtually determined by the extent of how close the  $\frac{R_v^k}{R_v^{\text{obs}}}$

(and  $\frac{R_v^0}{R_v^{\text{obs}}}$  for the clear part) gets to 1. An example of the ratio of the overcast

radiance and the observed radiance  $\frac{R_v^k}{R_v^{\text{obs}}}$  for each model level is given in Fig. 1 of

anna 2016-08-06 19:55



删除的内容: 7

GOES-Imager for the channel 5 ( $\sim 13.00 \mu m$ ). The clear sky radiance normalized by the observed radiance  $\frac{R_v^0}{R_v^{obs}}$  is also shown at the level 0 (Fig. 1). It is expected that the overcast radiance from the RTM decrease with the rising of the altitude. The cloud signal is strongest around level 5, where  $R_v^k$  fits  $R_v^{obs}$  most closely. The cloud retrievals depend not only on the basic input profiles (i.e., the overcast radiance on each level from RTM normalized by the observed radiance and the clear sky radiance from RTM normalized by the observed radiance) and but also on the algorithm applied for resolving the problem (e.g., MMR and PF in this study).

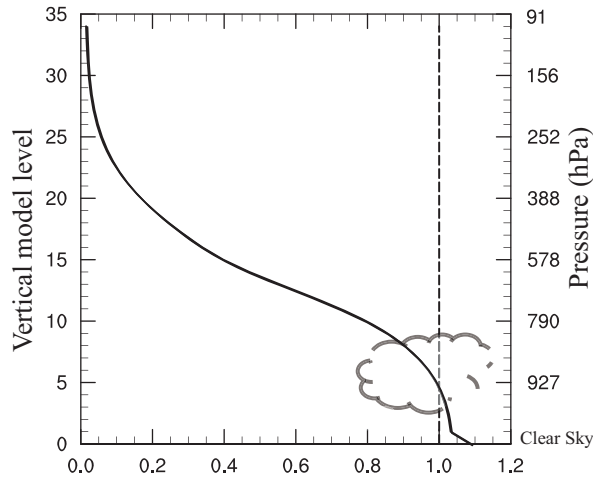


**Figure 1.** Ratio of the overcast radiances versus the observed radiance starting from the level 1. The ratio of the clear sky radiance normalized by the observed radiance corresponds to the level 0 (see text for explanation) for GOES-Imager for the channel 5. The approximate pressures corresponding to the model levels are also denoted.

To reveal the roles of various initial particles, Fig. 2a shows the weights for

different particles on the given FOV for channel 5 of GOES-Imager for the case shown in Fig. 1. Particles in Fig. 1 include one-layer cloud in group 2 described in section 2 with specified value of cloud fractions  $c^k$  (on the x-axis) on specified model levels  $k$  (on the y-axis) from 10% to 100% every 10%. With a fraction  $c^k$  of one-cloud layer at a given level  $k$  and a fraction of  $c^0 = 1 - c^k$  of clear sky, the simulated cloudy radiance can be denoted as  $R_v^{\text{cloud}} = c^k R_v^k + (1 - c^k) R_v^0$ . Hence the theoretical one-layer cloud fraction is solved as  $c^k = \frac{R_v^0 - R_v^{\text{obs}}}{R_v^0 - R_v^k}$  by fitting  $R_v^{\text{cloud}}$  to  $R_v^0$ . As expected, for one-layer cloud with full fraction,  $c^5$  equals to 100%. Since with the concept that  $R_v^k > R_v^{k+1}$ , no cloud can be present below level 5 since this would implies a  $R_v^{\text{cloud}}$  larger than the observation (or a  $c^i$  larger than 100%). It seems that clouds can be described by different possible states as particles with both large fractions and small fractions. Low clouds are easily estimated by one-layer cloud profile with large fractions (larger than 10%). The particles with small-fraction high clouds gain some weights to retrieve high clouds. The particle with the one-layer cloud on level 13 seems to gain least weight compared to the others levels. The weights for the particles with cloud fractions from 0% to 100% at the interval of 1% are also presented in Fig. 2b. By including more small-fraction one-layer clouds, the clouds around level 13 can be reproduced by the group of refined particles with 1% as the interval for approximate 10% cloud fractions. However, changing the level of the cloud for the fixed fraction (10%) does not seem to change the outgoing radiance much, probably due to the channel's low weight function peak (~750hPa).

The normalized  $J_0$  in Eq. (6) for different levels with a specific cloud fraction

Administrator 2016-08-22 17:02 ✓

删除的内容: of

Administrator 2016-09-10 15:24 ✓

删除的内容: of

Administrator 2016-08-08 11:06 ✓

带格式的: 字体: 倾斜

Administrator 2016-09-10 15:25 ✓

删除的内容: on the given FOV for channel 5 of GOES-Imager for the case shown in Fig. 1

Administrator 2016-08-11 10:35 ✓

带格式的: 字体颜色: 自动设置

Administrator 2016-08-08 11:13 ✓

删除的内容: by

from 0% to 100% every 10% are shown in the bottom panel of Fig. 3, with 10% and 1% as the intervals in Fig. 3c and Fig. 3d respectively. Here,  $J_o$  can be further derived as

$$J_o = r^2 \left( 1 - c^0 \frac{R_v^0}{R_{v,obs}} - c^k \frac{R_v^k}{R_{v,obs}} \right)^2 \quad (8),$$

with  $\sigma = \frac{R_v^{obs}}{r}$  and  $R_v^{cloud}(c^0, c^1, c^2, \dots, c^K) = c^0 R_v^0 + \sum_{k=1}^K c^k R_v^k$ .

From Fig. 3a, it is found that  $J_o$  is smallest around level-5 with 100% cloud fraction (denoted as 1 in legend) for the thin black line, with respect to the fact that the overcast radiance fits the observed radiance most closely for level-5 approximately. The grey line with 10% cloud fraction (0.1 in the legend) corresponds to the existence of a weight peak on level 19 in Fig. 2a. In addition, the gap between the grey line with 0.1 and the other lines from 0.2 to 1 explains why there's less continuity around level 13. Fig. 3b shows a similar pattern to Fig. 3a, except with densely-distributed  $J_o$  values around the level 13 from 0.1 to 1 in the legend. Those contiguous black lines in Fig. 3b are associated with the set of particles with cloud fractions from 10% to 100% at the interval of 1%.

Administrator 2016-09-10 15:25	✓	🔒
删除的内容: 2		
Administrator 2016-09-10 15:25	✓	🔒
删除的内容: 2		
Administrator 2016-09-10 15:25	✓	🔒
删除的内容: 2		

Administrator 2016-08-11 13:50	✓	🔒
删除的内容:		
Administrator 2016-09-10 15:25	✓	🔒
删除的内容: 2		
Administrator 2016-09-10 15:25	✓	🔒
删除的内容: c		

Administrator 2016-09-10 15:26	✓	🔒
删除的内容: 2d		
Administrator 2016-09-10 15:26	✓	🔒
删除的内容: 2c,		
Administrator 2016-09-10 15:26	✓	🔒
删除的内容: 2d		

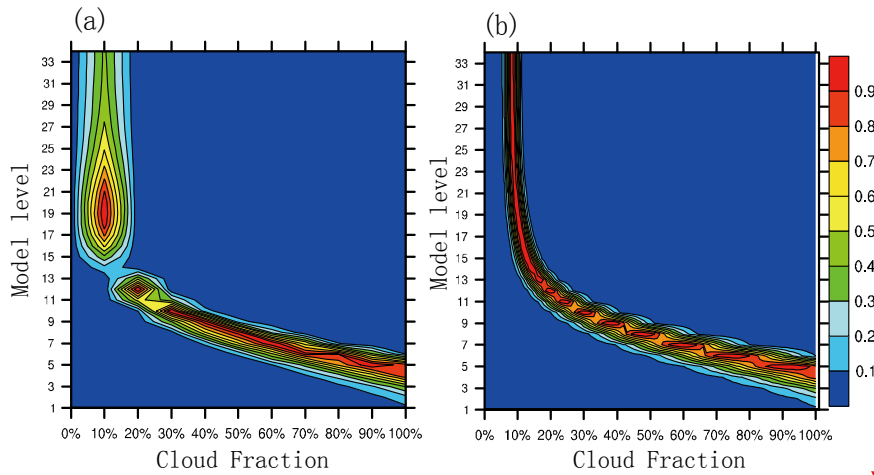


**Figure 2.** The weights for different particles with specified cloud fractions on the x-axis at one chosen model level shown on the y-axis from 0% to 100% (a) at the interval of 10% and (b) at the interval of 1%.

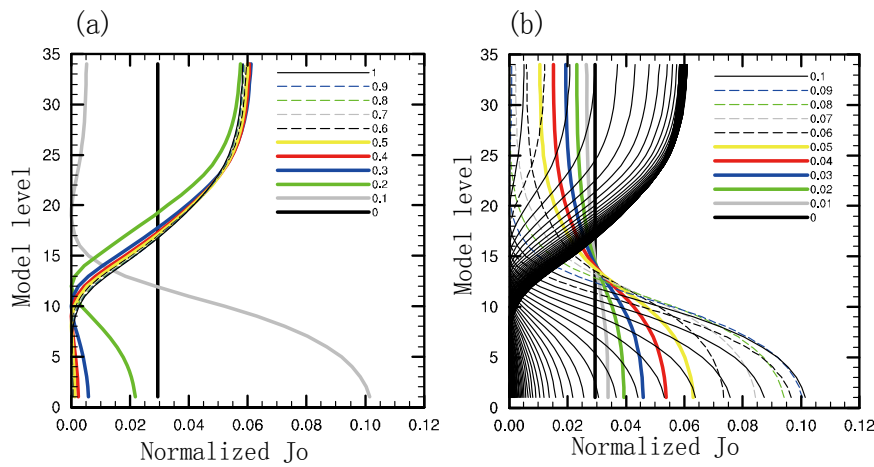
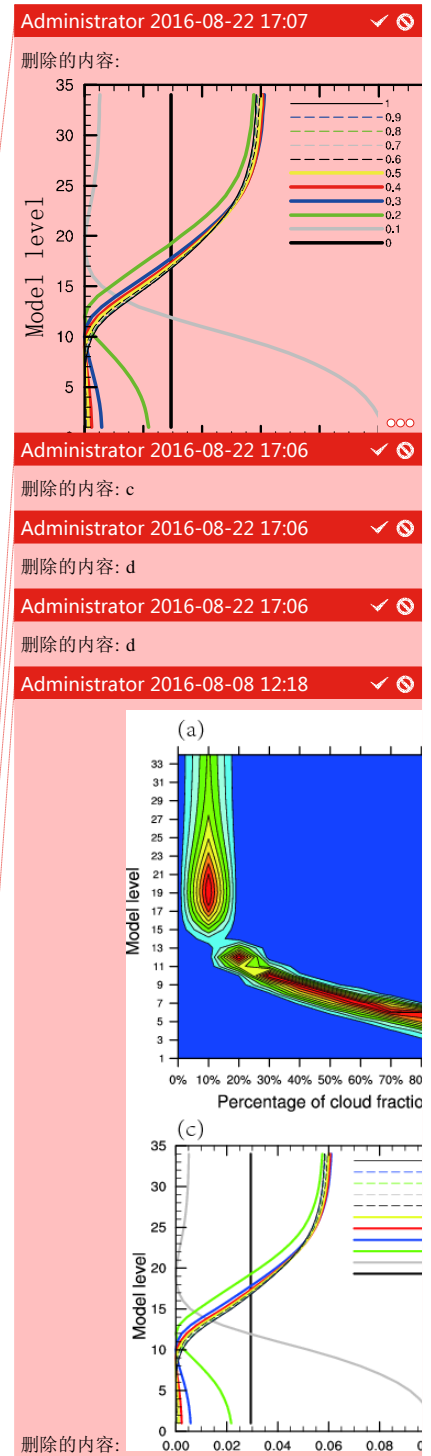


**Figure 3.** The normalized  $J_o$  (a) at the interval of 10% and (b) at the interval of 1%. In (b), the normalized  $J_o$  from 0.1 to 1 are all denoted as black lines.



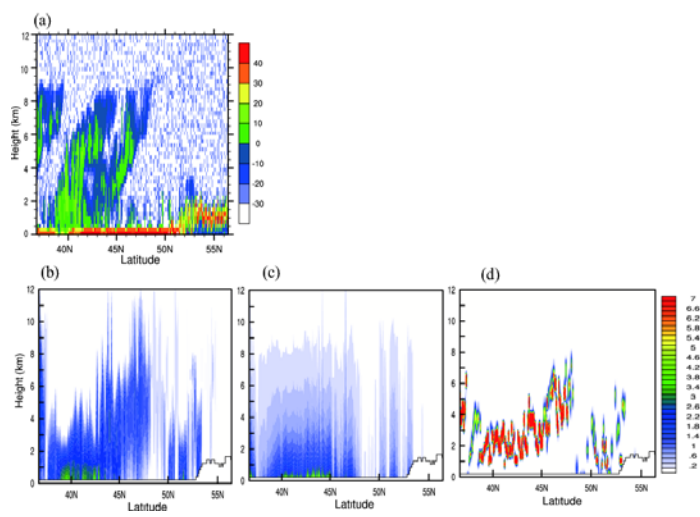
303 4.2 Cloud profiles

304 The retrieval experiments for a real case are conducted at 1100 UTC 3 June 2012  
305 when AIRS measurements and the CloudSat “2B-GEOPROF” products (Mace, 2004)  
306 are available. The vertical cross sections of the cloud fraction field of a real case are  
307 illustrated to further check how different collections of initial particles impact the  
308 retrieved cloud profiles. The standard radar reflectivity profiles from the CloudSat are  
309 shown in Fig. 4a as the validation source; Fig. 4b, Fig. 4c, and Fig. 4d show the cross  
310 sections of the cloud fractions along the CloudSat orbit tracks from the MMR, PF and  
311 APF experiments. The vertical structures of the clouds from MMR compare well with  
312 the radar reflectivity from CloudSat by retrieving the high clouds around 47N° and  
313 low clouds around 52N°. The PF experiment has difficulties in detecting the cloud  
314 tops appropriately. PF tends to detect a large quantity of low clouds; by adding a set of  
315 particles with small-fraction clouds in APF, higher clouds can be reproduced, which is  
316 consistent with the implications from Fig. 2b and 3b. APF detects clear strong cloud  
317 signals and removes the cloud fractions on near-surface levels around 36 N°  
318 successfully. Since the existences of ground-layer radar reflectivity are likely  
319 corresponding to the strong reflection from the underlying surface of the earth, the  
320 height of cloud bases of MMR and PF are not compared in this sub-section. The  
321 experiments with larger size of particles including 0% to 20% (at the interval of 1%)  
322 plus 30% to 100% (at the interval of 10%) or of 0% to 100% (at the interval of 1%)  
323 one-layer cloud profiles (introduced in section 2) yield similar results from APF but  
324 are much more costly (not shown).

Administrator 2016-09-10 15:27 ✓  
删除的内容: Figure 2. The weights for different particles with specified cloud fractions on the x-axis at one chosen model level shown on the y-axis from 0% to 100% (a) at the interval of 10% and (b) at the interval of 1%. The normalized  $J_0$  (c) at the interval of 10% and (d) at the interval of 1%. In (d), the normalized  $J_0$  from 0.1 to 1 are all denoted as black lines.

Administrator 2016-09-10 15:28 ✓  
删除的内容: 3  
Administrator 2016-09-10 15:28 ✓  
删除的内容: 3  
Administrator 2016-09-10 15:28 ✓  
删除的内容: 3  
Administrator 2016-09-10 15:28 ✓  
删除的内容: 3

Administrator 2016-09-10 15:28 ✓  
删除的内容: 2d



326

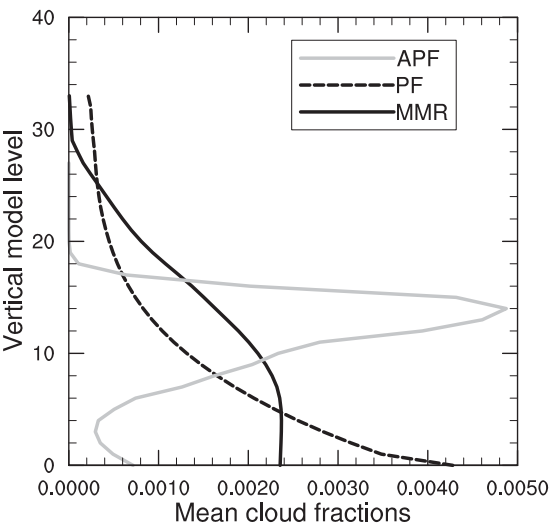
327 **Figure 4.** (a) The radar reflectivity (units: DBZ) cross sections from CloudSat, (b) the MMR  
328 retrieved cloud fractions (units: %) cross sections, (c) the PF retrieved cloud fractions, and (d) the  
329 APF retrieved cloud fractions valid at 1100 UTC 3 June 2012.

Administrator 2016-09-10 15:28 ✓  
删除的内容: 3

330 The vertical profiles of the averaged cloud fractions from MMR, PF, and APF are  
331 plotted in Fig. 5 at 1100 UTC 3 June 2012 with AIRS. Both MMR and PF  
332 experiments yield ambiguous cloud distributions, whereas APF retrieves much  
333 stronger cloud signals constrained between level-2 to level-20 (approximately from  
334 950hPa to 400hPa). More clouds around level 10 are retrieved (approximately 750hPa)  
335 in MMR, while PF is prone to retrieving clouds near surface levels. Note that MMR  
336 retrieves much higher cloud tops and lower cloud bases compared to APF. The cloud  
337 base from PF is lowest; the cloud top from MMR and PF is comparable. Only the  
338 APF related methods will be further discussed in later sections owing to the missing  
339 of high clouds using PF.

Administrator 2016-09-10 15:28 ✓  
删除的内容: 4

340



341

342 **Figure 5.** The mean cloud fraction on all model levels for the experiments MMR, PF, and APF

343 [with AIRS observations](#) valid at 1100 UTC 3 June 2012.

344 4.3 Cloud mask

345 Comparison experiments on real cases are further performed for over longer time  
346 period from 0000 UTC 12 December 2013 to 0700 UTC 12 December 2013. The  
347 cloud mask is marked as cloudy when there is a recognizable existence of cloud on  
348 any level from MMR or PF retrievals. Both the NASA GOES Imager products and the  
349 MMR-retrieved fields are interpolated to the same  $0.1^{\circ}\times0.1^{\circ}$  latitude–longitude grid

350 with 0 for clear and 1 for cloudy before the comparisons for verification. Fig. 6 shows  
351 the *hits*, *false\_alarms* and *misses* locations with the use of [GOES-Imager](#), MODIS,  
352 CrIS, AIRS, and IASI [radiances](#) in the retrieval algorithms at 0700 UTC 12 December  
353 2013. Note that, cloud mask retrievals from both the MMR and APF hit the clear and  
354 cloudy events well in Fig. 6a and 6b. In most areas, the MMR experiment

Administrator 2016-09-10 15:29	✓	🔒
删除的内容: 4		
anna 2016-08-06 08:35	✓	🔒
删除的内容: from		

Administrator 2016-09-10 15:29	✓	🔒
删除的内容: 5		
anna 2016-08-06 08:39	✓	🔒
删除的内容: radiances from		
Administrator 2016-09-10 15:29	✓	🔒
删除的内容: 5		
Administrator 2016-09-10 15:29	✓	🔒
删除的内容: 5		



355 overestimated the cloud mask with more false alarm events compared to the APF  
356 experiment, since the MMR solution is an “overly smoothed” estimation of the true  
357 vertical profile. It seems that the accuracy of cloud detection is lower for areas with  
358 high altitude than under tropical conditions, indicating that the smaller lapse rate in  
359 the atmosphere will lead radiance less sensitivity to clouds over polar areas. Fig. 6c  
360 shows the cloud mask results from the APFg2 experiment without the perturbed  
361 particles in group-1 introduced in section 2. There is no large discrepancy between  
362 Fig. 6b and Fig. 6c, suggesting that the particles in group-2 that fully span the  
363 possibility of the cloud distributions, are more determinant in retrieving the cloud  
364 mask.

365

Administrator 2016-09-10 15:29 ✓ 删除的内容: 5

Administrator 2016-09-10 15:30 ✓ 删除的内容: 5

Administrator 2016-09-10 15:30 ✓ 删除的内容: 5

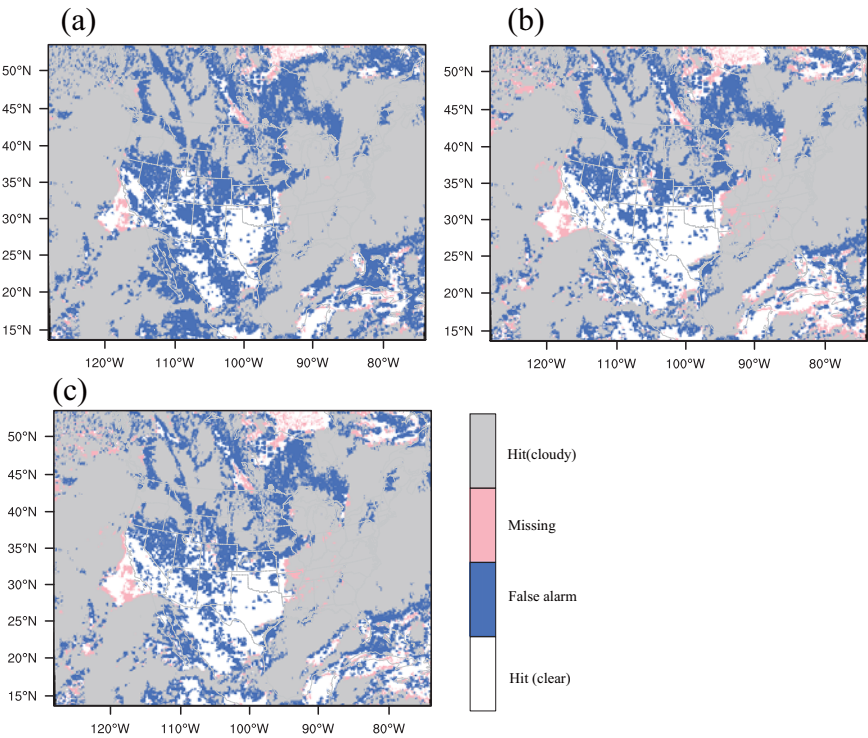


**Figure 6.** The false alarms, misses, and hits for clear and cloudy event locations with (a) the MMR method, (b) the APF method, and (c) the APF method but without the group-1 particles (see text for detailed explanations) valid at 0700 UTC 15 December 2013.

Administrator 2016-09-10 15:30 ✓  
删除的内容: 5

#### 4.4 Cloud top and base pressure

The retrieved cloud top pressures (CTP) and cloud bottom pressures (CBP) from this study along with the NASA GOES cloud products are illustrated in Fig. 7. The CTPs from both methods are in good accordance with the NASA cloud products for high clouds (from 100 hPa to 600 hPa) in Fig. 7a, 7c, and 7e. The retrieved cloud top heights from MMR are overall higher than those from the NASA reference, especially for lower clouds at approximately 750-1000 hPa (e. g., between longitude -100° and -90°). On the other hand, the CTPs from APF are much closer to those in the reference for both high and low clouds. APF overestimates the CBPs for some low clouds (putting the clouds too low) in Fig. 7f; the overestimation of the CBP is even more obvious from MMR in most regions in Fig. 7d.

Administrator 2016-09-10 15:31 ✓  
删除的内容: 6

Administrator 2016-09-10 15:31 ✓  
删除的内容: 6

Administrator 2016-09-10 15:31 ✓  
删除的内容: 6

Administrator 2016-09-10 15:31 ✓  
删除的内容: 6

Administrator 2016-09-10 15:31 ✓  
删除的内容: 6

Administrator 2016-09-10 15:31 ✓  
删除的内容: 6

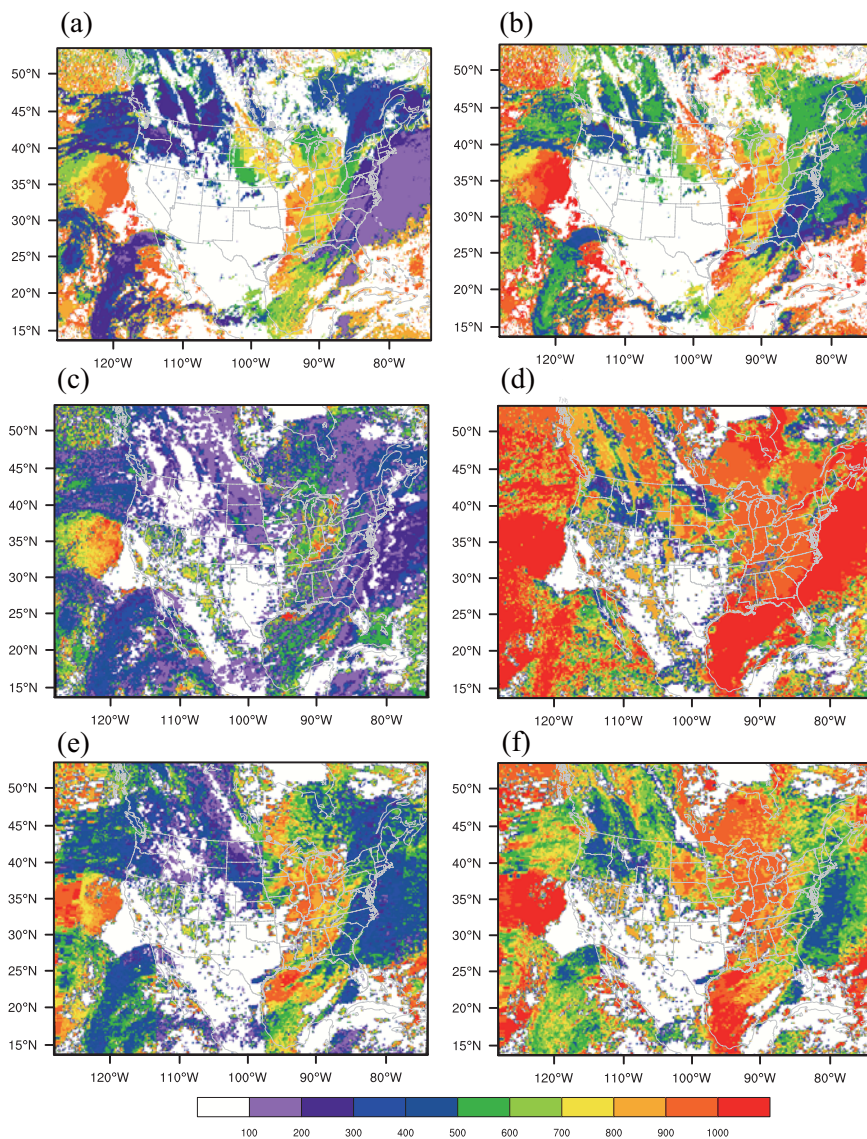


**Figure 7.** The cloud top pressure (left panels) from (a) the NASA GOES retrieval, (c) the MMR method, (e) the APF method, and the cloud bottom pressure (right panels) from (b) the NASA GOES retrieval, (d) the MMR method, (f) the APF method valid at 0700 UTC 15 December 2013.

The CTPs from NASA GOES cloud products for more hours (0300UTC, 0500UTC, 0700UTC) together with the independent CTP retrievals from MODIS

Administrator 2016-09-10 15:32



删除的内容: 6



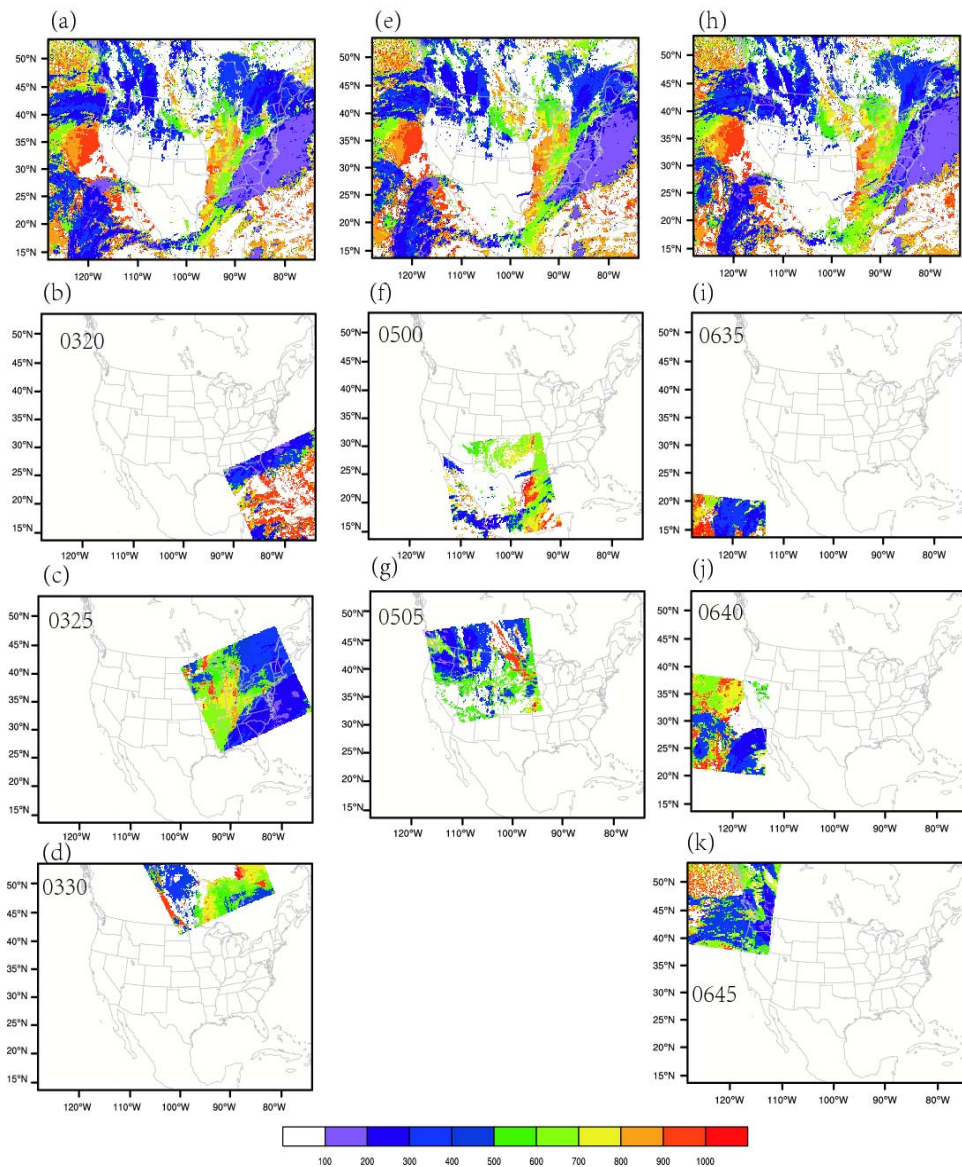


**Figure 8.** The cloud top pressure for (a) 0300UTC from the GOES NASA retrieval, (b) 0320UTC, (c) 0325UTC, (d) 0330UTC from MODIS level-2 products; (e) 0500UTC from the GOES NASA retrieval, (f) 0500UTC, (g) 0505UTC; (h) 0700UTC from the GOES NASA retrieval, (i) 0635UTC, (j) 0640UTC, and (k) 0645UTC from MODIS level-2 products.

Administrator 2016-09-10 15:33



删除的内容: 7

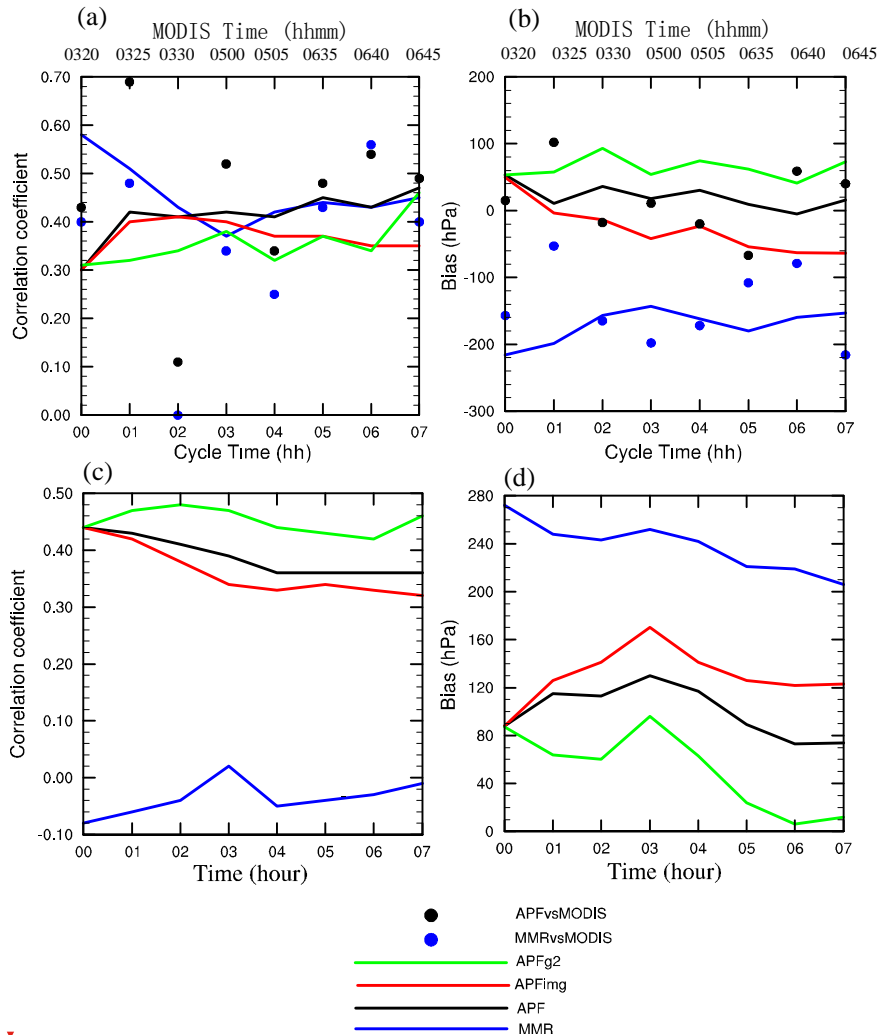


Fig. 9 presents the correlation coefficients and biases of the CTP and CBP verified against the NASA GOES and MODIS retrievals. The solid lines denote the results regarding the CTP and CBP versus the NASA GOES products from 0000 UTC to 0700 UTC, while the dots describe the CTP results versus the cloud top retrievals in NASA MODIS level-2 products at 0320UTC, 0325UTC, 0330UTC, 0500UTC, 0505UTC, 0635UTC, 0640UTC, and 0645UTC. Here the negative bias means that the retrieved clouds are higher than the reference. Vice versa, the positive bias indicates the clouds are put too low. We conducted another experiment “APFing” that applies solely GOES Imager data to check the added value from the high spectral resolution radiances (such as, CrIS, AIRS, and IASI). In Fig. 9a, the correlations between the retrievals from MMR and the NASA GOES retrievals are comparable with from APF for most hours; APF gains overall higher correlations with the CTPs in the MODIS retrievals. From the bias in Fig. 9b, it seems that the CTPs from MMR are underestimated (putting the clouds too high) consistently against both retrievals with GOES and MODIS radiances. Fig. 9c shows that the correlations are weaker for MMR compared to others all the time. In Fig. 9d, the positive CBP biases from MMR are remarkable, while the CBP biases from APF are largely reduced. Generally, APFing degrades the CTP and CBP results consistently, suggesting that radiances with high spectral resolutions are able to improve the vertical descriptions of cloud profiles. It is found that the clouds retrieved with APFg2 are shrunken in terms of cloud depth with notably lower cloud top and higher cloud base compared to APF, when excluding the perturbed particles in the first group.

Administrator 2016-09-10 15:33 ✓  
删除的内容: 8

Administrator 2016-09-10 15:33 ✓  
删除的内容: 8

Administrator 2016-09-10 15:33 ✓  
删除的内容: 8  
anna 2016-08-06 08:40 ✓  
删除的内容: from  
Administrator 2016-09-10 15:33 ✓  
删除的内容: 8  
Administrator 2016-09-10 15:34 ✓  
删除的内容: 8



**Figure 2.** (a) Correlation coefficient, (b) bias for the cloud top pressure, (c) correlation coefficient, and (d) bias for the cloud bottom pressure versus the NASA GOES retrievals from 0600 UTC 15 December 2013 to 0700 UTC 15 December 2013. Black and blue dots denote results versus the MODIS level-2 cloud top pressure retrieval valid at 0320UTC, 0325UTC, 0330UTC, 0500UTC, 0505UTC, 0635UTC, 0640UTC, and 0645UTC. The valid times for the MODIS level-2 data are shown on the top of the x-axis.

Administrator 2016-08-08 12:20 ✓

删除的内容:

Administrator 2016-09-10 15:34 ✓

删除的内容: 8

429 4.5 Computational issues

430 Fig. 10a represents the elapsed times for the MMR and APF experiments and the  
431 counts of radiance observations in use are shown in Fig. 10b from 0000 UTC to 0700  
432 UTC 12 December 2013. The profile of computing time in MMR is quite different  
433 from that in PF. The cost of MMR is dominated by the heavy minimization procedure,  
434 while APF is more associated with the processes of initializing particles and  
435 calculating weights for all the particles. The computing times were measured from  
436 cloud retrieving runs with 64 MPI-tasks on a single computing node in an IBM  
437 iDataPlex Cluster. The measured wall clock computing times show that generally  
438 MMR is computationally more expensive for most of the time than APF. It seems the  
439 wall clock times for MMR are generally proportional to the data amount used. While  
440 for the APF experiment, the wall clock time is mostly determined by the particles size  
441 and partly affected by the channel number, such as for 2013121202 and 2013121206,  
442 when the total counts of the hyperspectral sensors (IASI, CrIs, and AIRS) are large.  
443 The PF experiments using particles of one-layer cloud with 100% cloud fractions  
444 usually take less than 5 minutes for the same periods (not shown).

Administrator 2016-09-10 15:34	✓	🔒
删除的内容: 9		
Administrator 2016-09-10 15:34	✓	🔒
删除的内容: 9		



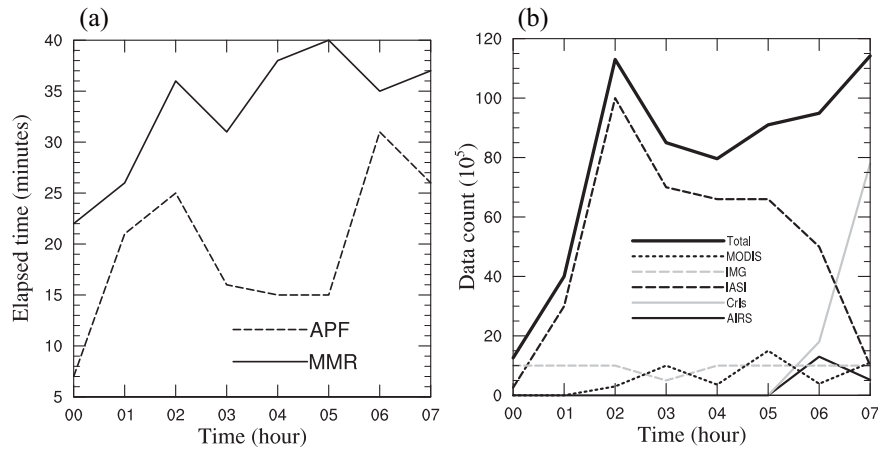


**Figure 10.** (a) The elapsed time and (b) the data count from 0000 UTC to 0700 UTC 15 December

Administrator 2016-09-10 15:34



删除的内容: 9

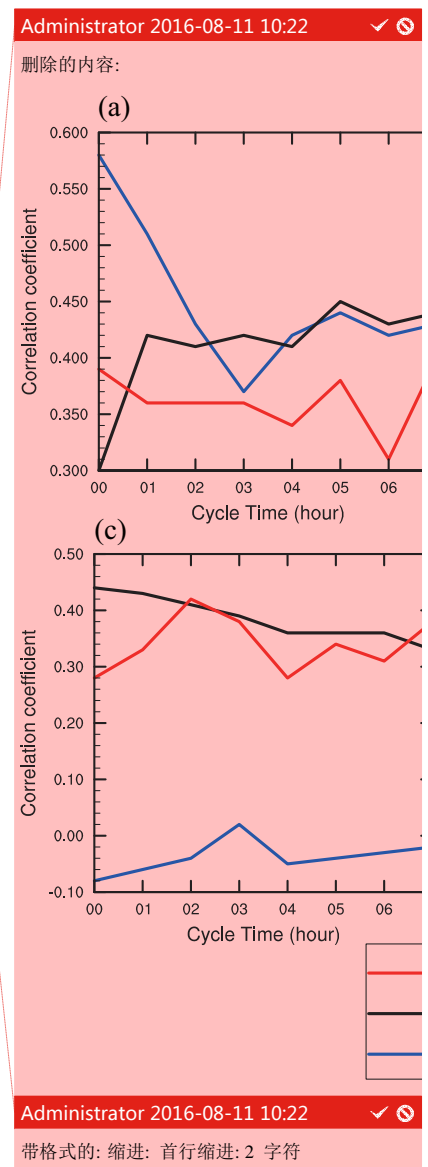
#### 4.6 Resolving the filtering problem on model grids

As explained in subsection 3.3, the filtering problem is resolved in the radiance observational space at each FOV of each sensor independently and sequentially. For each FOV, the retrieved cloud fractions are extrapolated to its neighboring model grid points afterwards. We order the sensors in the cloud retrieving procedure as GOES-Imager, MODIS, CrIS, AIRS, and IASI, aiming to optimize the vertical clouds using sensors featured with sufficient spectral resolutions. As a consequence, the retrievals from the last sensor determine the final output to the most extent, causing the cloud retrievals highly subjective to the ordering of the sensors. On the other hand, it means the information from other prior sensors will be more or less discarded. In this section, a different way of resolving the filtering problem is preliminarily tested, in which the weights for each particle are aggregated over all available sensors by

460 calling the forward radiative transfer model on neighbouring model grids.

461 Fig. 1 shows the clouds retrievals from the grid-based method. It is noted that  
462 the grid-based scheme yields slightly worse results of CTP and neutral results of CBP  
463 compared with those from the observation-based (FOV-based) scheme, indicating that  
464 the hyperspectral sensors probably favor the retrieved CTP and CBP in the  
465 FOV-based scheme, which are available for most of the time. It is worth pointing out  
466 that the ordering of different sensors has nearly no effect on the final cloud retrievals,  
467 when the weights of the particles are calculated in model space (not shown). The final  
468 cloud retrieval is no longer overwritten by the retrieval from the last sensor but is a  
469 total solution with all the sensors fairly considered, instead. The computational cost of  
470 retrieving clouds in model space is comparable or slightly heavier than that in  
471 observation space. The computational cost of the grid-based scheme scales with the  
472 number of the computing nodes more directly, compared to that of the FOV-based  
473 scheme.

Administrator 2016-09-10 15:34 ✓  
删除的内容: 0



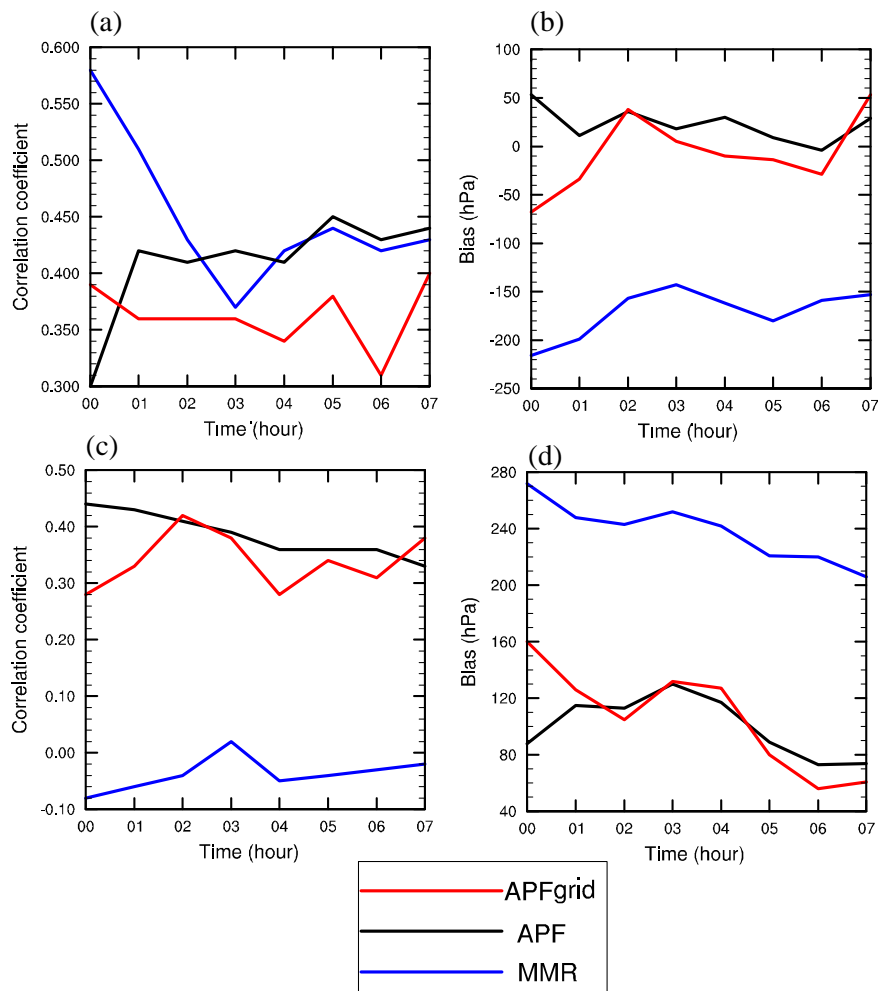


**Figure 1.** (a) Correlation coefficient, (b) bias for the cloud top pressure, (c) correlation coefficient, and (d) bias for the cloud bottom pressure versus the NASA GOES retrievals from 0000 UTC to 0700 UTC 15 December 2013.

## 5. Discussion and conclusion

Administrator 2016-09-10 15:34

删除的内容: 0

479        This study presents a new cloud retrieval method based on the particle filter (PF)  
480        in the framework of GSI, as a competitive alternative to the MMR method. The  
481        behaviors of different particle initializations are demonstrated on one single field of  
482        view and the CONUS domain respectively. Comparisons between the PF and the  
483        MMR method are conducted in terms of the features of cloud mask, cloud top, cloud  
484        base, and the vertical distributions of clouds. It was found that the PF method  
485        retrieves clear cloud signals while MMR is more ambiguous in detecting clouds. By  
486        adding more small-fraction particles, high clouds can be better interpreted. From the  
487        statistical results, it was found that MMR underestimates the cloud top pressures (put  
488        the clouds top too high) and overestimates the cloud bottom pressures (put the clouds  
489        top too low) as well. APF improves both the retrievals of cloud tops and cloud bases  
490        remarkably, especially for the cloud bases. As expected, radiances with high spectral  
491        resolutions contribute to quantitative cloud top and cloud base retrievals. In addition,  
492        a different way of resolving the filtering problem over each model grid is tested to  
493        aggregate the weights with all available sensors considered, which is proven to be less  
494        constrained by the ordering of sensors. Last but not least, the PF method is overall  
495        more computationally efficient; the cost of the model grid-based PF method scales  
496        more directly with the number of the computing nodes.

497        In future work, validation studies using multispectral imagers on geostationary  
498        satellites, spaceborne lidars (or radar), and surface site data will continue, and the  
499        results will be used to update the retrieval algorithm. Maximizing the consistency in  
500        the products across platforms and optimizing the synergistic use of multiple-source

501 radiances in the new algorithm are important aspects. To estimate the flow dependent  
502 uncertainties in the cloud analysis and in the forecasts, the ensemble nowcasting with  
503 three dimensional cloud fractions via the rapid-update cycling mode is also planned.  
504 [Increasing the highest extent cloudy cases will be included in future studies.](#) Finally,  
505 the use of cloud liquid water and ice mixing ratios retrieved from the cloud fractions  
506 using multi-sensor radiances to pre-process the first guess in numerical weather  
507 forecast is another promising application.

#### 508 **Code and/or data availability**

509 The MMR cloud retrieval codes can be obtained freely from  
510 (<http://www2.mmm.ucar.edu/wrf/users/wrfda/>). The other codes can be obtained by  
511 emails from the authors.

#### 512 **Acknowledgments**

513 This work was jointly sponsored by the the US Air Force Weather Agency under the  
514 project "Air Force Coupled Analysis and Prediction System", Natural Science  
515 Foundation of Jiangsu Province under Grant No BK20160954, the 973 Program  
516 (Grant No. 2013CB430102), the Beijige Funding from Jiangsu Research Institute of  
517 Meteorological Science (BJG201510), the National Natural Science Foundation of  
518 China (41375025), and the Priority Academic Program Development of Jiangsu  
519 Higher Education Institutions (PAPD). The authors would like to thank Chris Davis  
520 for fruitful discussions, and to Bobbie Weaver for editing the manuscript. We greatly  
521 thank the anonymous reviewers for their valuable comments on the earlier versions of  
522 the manuscript.

## REFERENCES

- Ackerman, S. A., K. I. Strabala, W. P. Menzel, R. A. Frey, C. C. Moeller, and L. E. Gumley: Discriminating clear sky from clouds with MODIS, *Geophys. Res. Atmos.*, 103, 32141-32157, 1998.
- Auligné, T., Lorenc, A., Michel, Y., Montmerle, T., Jones, A., Hu, M., and Dudhia, J.: Toward a New Cloud Analysis and Prediction System, *B Am Meteorol Soc*, 92, 207-210, 2011.
- Auligné, T.: Multivariate minimum residual method for cloud retrieval. Part I: Theoretical aspects and simulated observation experiments, *Monthly Weather Review*, 142, 4383-4398, 2014a.
- Auligné, T.: Multivariate minimum residual method for cloud retrieval. Part II: Real observations experiments, *Monthly Weather Review*, 142, 4399-4415, 2014b.
- Aumann, H. H., Chahine, M. T., Gautier, C., Goldberg, M. D., Kalnay, E., McMillin, L. M., Revercomb, H., Rosenkranz, P. W., Smith, W. L., and Staelin, D. H.: AIRS/AMSU/HSB on the Aqua mission: Design, science objectives, data products, and processing systems, *Geoscience and Remote Sensing, IEEE Transactions on*, 41, 253-264, 2003.
- Bayler, G. M., Aune, R., and Raymond, W.: NWP cloud initialization using GOES sounder data and improved modeling of nonprecipitating clouds, *Monthly weather review*, 128, 3911-3920, 2000.
- Berrocal, V. J., Raftery, A. E., and Gneiting, T.: Combining spatial statistical and ensemble information in probabilistic weather forecasts, *Monthly Weather Review*, 135, 1386-1402, 2007.
- Blumstein, D., Chalon, G., Carlier, T., Buil, C., Hebert, P., Maciaszek, T., Ponce, G., Phulpin, T., Tournier, B., and Simeoni, D.: IASI instrument: Technical overview and measured performances, *Optical Science and Technology, the SPIE 49th Annual Meeting*, 2004, 196-207,
- Brückner, M., Pospichal, B., Macke, A., and Wendisch, M.: A new multispectral cloud retrieval method for ship - based solar transmissivity measurements, *Journal of Geophysical Research: Atmospheres*, 119, 2014.
- Descombes, G., Auligne, T., and Lin, H.-C., Xu, D., Schwartz, C. S., Vandenberghe, F.: Multi-sensor Advection Diffusion nowCast (MADCast) for cloud analysis and short-term prediction., *NCAR Technical Note NCAR/TN-509+STR*, , 21 pp., 2014.
- Eyre, J. R., and Menzel, W. P.: Retrieval of cloud parameters from satellite sounder data: A simulation study, *Journal of Applied Meteorology*, 28, 267-275, 1989.
- Han, Y., Delst, P. V., Liu, Q., Weng, F., Yan, B., Treadon, R., and Derber, J.: JCSDA Community Radiative Transfer Model (CRTM)—Version 1, *NOAA Tech. Rep. NESDIS*, 122, 33, 2006.
- Hu, M., Xue, M., and Brewster, K.: 3DVAR and Cloud Analysis with WSR-88D Level-II Data for the Prediction of the Fort Worth, Texas, Tornadoic Thunderstorms. Part I: Cloud Analysis and Its Impact, *Monthly Weather Review*, 134, 675-698, 10.1175/mwr3092.1, 2006.

Huang, H.-L., Smith, W. L., Li, J., Antonelli, P., Wu, X., Knuteson, R. O., Huang, B., and Osborne, B. J.: Minimum local emissivity variance retrieval of cloud altitude and effective spectral emissivity-simulation and initial verification, *Journal of applied meteorology*, 43, 795-809, 2004.

Karlsson, K.-G., Johansson, E., and Devasthale, A.: Advancing the uncertainty characterisation of cloud masking in passive satellite imagery: Probabilistic formulations for NOAA AVHRR data, *Remote Sensing of Environment*, 158, 126-139, 2015.

Kleist, D. T., Parrish, D. F., Derber, J. C., Treadon, R., Wu, W. S., and Lord, S.: Introduction of the GSI into the NCEP Global Data Assimilation System, *Weather and Forecasting*, 24, 1691-1705, 10.1175/2009waf2222201.1, 2009.

Liu, Q., and Weng, F.: Advanced doubling-adding method for radiative transfer in planetary atmospheres, *Journal of the atmospheric sciences*, 63, 3459-3465, 2006.

Mace, G. G., 2004: Level 2 GEOPROF product process description and interface control document (v.3): Level 2 GEOPROF product process description and interface control document (v.3), Tech. rep., CIRA, Colorado State University, 2004.

Mechri, R., Ottlé, C., Pannekoucke, O., and Kallel, A.: Genetic particle filter application to land surface temperature downscaling, *Journal of Geophysical Research: Atmospheres*, 119, 2131-2146, 2014.

Menzel, W., Smith, W., and Stewart, T.: Improved cloud motion wind vector and altitude assignment using VAS, *Journal of Climate and Applied meteorology*, 22, 377-384, 1983.

Menzel, W. P., and Purdom, J. F.: Introducing GOES-I: The first of a new generation of geostationary operational environmental satellites, *B Am Meteorol Soc*, 75, 757-781, 1994.

Platnick, S., King, M. D., Ackerman, S. A., Menzel, W. P., Baum, B. A., Riédi, J. C., and Frey, R. A.: The MODIS cloud products: Algorithms and examples from Terra, *Geoscience and Remote Sensing, IEEE Transactions on*, 41, 459-473, 2003.

Rossow, W. B., and Schiffer, R. A.: ISCCP cloud data products, *B Am Meteorol Soc*, 72, 2-20, 1991.

Rossow, W. B., Walker, A. W., and Garder, L. C.: Comparison of ISCCP and other cloud amounts, *Journal of Climate*, 6, 2394-2418, 1993.

Shen, Z. Q., and Tang, Y. M.: A modified ensemble Kalman particle filter for non-Gaussian systems with nonlinear measurement functions, *J Adv Model Earth Sy*, 7, 50-66, 2015.

Skamarock, W., C., Klemp, J. B., Dudhia, J., Gill, D. O., Barker, D. M., Duda, G., Huang, X.-Y., Wang, W., and Powers, J. G.: A description of the Advanced Research WRF version 3., *NCAR*, 113, 2008.

Smith, A., Atkinson, N., Bell, W., and Doherty, A.: An initial assessment of observations from the Suomi - NPP satellite: data from the Cross - track Infrared Sounder (CrIS), *Atmospheric Science Letters*, 16, 260-266, 2015.

Snyder, C., and Zhang, F. Q.: Assimilation of simulated Doppler radar observations with an ensemble Kalman filter, *Monthly Weather Review*, 131, 1663-1677, Doi

10.1175//2555.1, 2003.

Stephens, G. L., Vane, D. G., Boain, R. J., Mace, G. G., Sassen, K., Wang, Z., Illingworth, A. J., O'Connor, E. J., Rossow, W. B., and Durden, S. L.: The CloudSat mission and the A-Train: A new dimension of space-based observations of clouds and precipitation, *B Am Meteorol Soc*, 83, 1771-1790, 2002.

van Leeuwen, P. J.: Nonlinear data assimilation in geosciences: an extremely efficient particle filter, *Quarterly Journal of the Royal Meteorological Society*, 136, 1991-1999, 2010.

Wu, W.-S., Purser, R. J., and Parrish, D. F.: Three-dimensional variational analysis with spatially inhomogeneous covariances, *Monthly Weather Review*, 130, 2905-2916, 2002.

Wu, X., and Smith, W. L.: Assimilation of ERBE data with a nonlinear programming technique to improve cloud-cover diagnostics, 120, 2009-2004, 1992.

Xu, D., Auligné, T., and Huang, X.-Y.: A Retrieval Method for 3-D Cloud Parameters Using Radiance Observations from Multiple Satellites, *Advances in atmospheric physics*, 32, 349-362, 2015.

Xu, D. M., Liu, Z. Q., Huang, X. Y., Min, J. Z., and Wang, H. L.: Impact of assimilating IASI radiance observations on forecasts of two tropical cyclones, *Meteorology and Atmospheric Physics*, 122, 1-18, 10.1007/s00703-013-0276-2, 2013.

Zhao, C., Xie, S., Klein, S. A., Protat, A., Shupe, M. D., McFarlane, S. A., Comstock, J. M., Delanoë, J., Deng, M., and Dunn, M.: Toward understanding of differences in current cloud retrievals of ARM ground - based measurements, *Journal of Geophysical Research: Atmospheres*, 117, 2012.